Journal of Volcanology and Geothermal Research 453 (2024) 108148

Contents lists available at ScienceDirect

Journal of Volcanology and Geothermal Research

journal homepage: www.journals.elsevier.com/journal-of-volcanology-and-geothermal-research

Deep-seated gravity instability of the southern apron of the Ischia volcanic island (Tyrrhenian Sea, Italy)

Giovanni de Alteriis [a,*], Crescenzo Violante [b], Fabrizio Pepe [c]

[a] ISMAR, Istituto di Scienze Marine, CNR, Napoli, Italy
[b] ISPC, Istituto di Scienze del Patrimonio Culturale, CNR, Napoli, Italy
[c] Dipartimento di Scienze della Terra e del Mare (DiSTeM), Università di Palermo, Italy

ARTICLE INFO

Keywords:
Ischia island
Deep-seated slump
Submarine landslide
Volcano-spreading

ABSTRACT

Ischia Island is an active volcano representing the emerged sector of an *E*-W trending volcanic ridge largely extending undersea. Its collapsing behaviour, mainly in the form of fast-moving, terrestrial and submarine debris avalanches, has been recognized during the Holocene, but much less is known about previous gravity-driven processes. Using high-resolution multibeam bathymetric data and seismic reflection profiles, we provide evidence that the Island's southwestern flank has been involved in a slow-moving, deep-seated slope deformation that has displaced large volumes of its apron since the Late Pleistocene and until very recent or contemporary times. A long tongue of deformed seafloor, spreading up to 45 km from the Island over an area of 330 km^2, between 500 and 1300 m water depths, has been detected along its southwestern slope. Different types of mass movements, genetically associated with each other, characterize this landslide: 1) a basal slump anticline, corresponding to a bulge on the bathymetry detaching at about 400 m sub-bottom depth; 2) an intermediate-mass movement chiefly consisting of debris avalanches and debris/turbiditic flows; 3) an upper mass movement consisting of hundred-metre size slumps detaching at relatively shallow depths. Conservative estimates indicate that at least 50 km^3 of volcano-clastic and hemipelagic deposits have been mobilized, most of which comprise the basal slump anticline. This submarine landslide can be explained as a gravity failure of the continental slope unrelated to volcanism or rather as a process related to the dynamics of the volcanic edifice, which would imply volcano-spreading.

1. Introduction

Submarine landslides affecting continental margins include a wide range of downslope movement of sediment or rock under the effect of gravity, from extremely rapid, flow-like debris on steep slopes to slow-moving, rotational slumps. Their volumes vary by several orders of magnitude, with the most significant known cases attaining thousands of km^3 of sediments (see review in Masson et al., 2006). Similar mass movements have been increasingly recognized in volcanic settings from large, hot-spot-related oceanic islands (Moore et al., 1994) to smaller, andesitic islands or coastal volcanoes mainly in the form of fast volcanic debris avalanches and, less frequently, as deep-seated mass movements occurring over much longer (10^3–10^5 y) timescales (see in Mitchell et al., 2002 and references therein). In the past decades, these long-term gravity-driven deformation processes have been identified at several oceanic and coastal volcanoes, for instance, the southern flank of Kilauea (Denlinger and Okubo, 1995); the eastern flanks of Mt. Etna and Piton de la Fournaise (Borgia et al., 2000; Poland et al., 2017) or the western flank of Cumbre Vieja volcano (González et al., 2010). Gravitational stresses acting on a volcanic edifice can lead to gradual relaxation associated with summit subsidence and flank bulging and/or displacement along the volcano's base (e.g. Morgan et al., 2000; Morgan et al., 2007).

The relationships between gravitational loading and the characteristics of volcanic edifice deformation and flank displacement have been modelled in laboratories, showing the role of low strength, ductile layers located at or below the base of the volcano (Delaney et al., 1998; Oehler et al., 2005; Delcamp et al., 2008; Delcamp et al., 2012; Le Corvec and Walter, 2009). Analogue and numerical models also indicate that motion along a basal detachment zone (or 'décollement') produces a range of structures, including grabens, troughs, en échelon faults, folds and thrusts. These structures were interpreted as the results of two different

* Corresponding author.
E-mail address: giovanni.dealteriis@cnr.it (G. de Alteriis).

https://doi.org/10.1016/j.jvolgeores.2024.108148
Received 22 September 2023; Received in revised form 28 July 2024; Accepted 30 July 2024
Available online 5 August 2024

long-term deformations: volcano spreading (Borgia et al., 1992) and volcano sagging. These long-term deformation were initially envisaged for some Martian volcanoes (Byrne et al., 2013), or by some combination of spreading and sagging (Borgia and van Wyk de Vries, 2003; Kervyn et al., 2014; McGovern et al., 2015). Volcano spreading is characterized by slow outward flank displacement along a basal décollement with the production of normal or strike-slip faults on the volcanic edifice and folds and thrusts at or beyond the edifice's base that accommodates the extension of the volcano flanks. Volcano sagging implies a flexural behaviour of the lithosphere under the volcano basement. It generates a contractional stress field in the central area of the edifice marked by imbricated terraces and folds encircled by peripheral extension characterized by roughly concentric extensional faults. Sagging and spreading models imply a low-strength, ductile layer underlying the relatively brittle volcanic edifice and its upper basement. The progressive transition from sagging to spreading during the volcano growth has been recently modelled in analogue experiments and hypothesized for some cases in nature (Holohan et al., 2023). According to these models, sagging to spreading behaviour depends on the ratio between the brittle and ductile thicknesses and the height of the volcanic edifice.

Ischia Island is an active volcanic complex developed in the eastern sector of the Tyrrhenian Sea whose early activity dates back to 150 ka at least (Gillot et al., 1982). It represents the emerged portion of an *E*-W trending ridge extending from the Campanian continental slope to the Campi Flegrei volcanic field. One of the peculiarities of the Island's recent volcanic evolution is the volcano-tectonic uplift of Mt. Epomeo, its central relief, widely recognized as a resurgent block inside a previous caldera depression (Orsi et al., 1991). Such uplift has favoured periodic flank collapses involving the caldera structure (Tibaldi and Vezzoli, 2004) and generating, during the Holocene, both terrestrial (Della Seta et al., 2012) and submarine landslides mainly in the form of fast debris flows and debris avalanches (de Alteriis and Violante, 2009) that have accompanied constructional volcanism. At the same time, an increasing number of recent investigations, based on ground levelling surveys or radar satellite interferometry (Manzo et al., 2006; Castaldo et al., 2017), are revealing a long-term subsidence process that involves most part or probably the entire Island and which is not biased by local, shallow landslides. Whether this subsidence is a transient phenomenon, confined to the former caldera area or instead can be related to a deep-seated process involving the entire volcanic edifice is an issue of great interest that can best be addressed with the contribution of marine geophysical data over the undersea volcano basement.

This paper aims to contribute to understanding the above phenomena by providing a range of recently discovered marine geophysical evidence. Data and interpretations we present document, for the first time, the internal and external geometries of an outstanding, large-scale submarine landslide observed off Ischia southwestern flank. The dataset includes unpublished bathymetric and marine geophysical data and gravity core samples. The investigated area highlights the recent volcanological history of Ischia. Also, it can be considered a natural laboratory to investigate the mechanisms that promote the gravitational instability of volcanic edifices.

2. Geo-volcanologic setting

The study area belongs to the Eastern Tyrrhenian margin off the

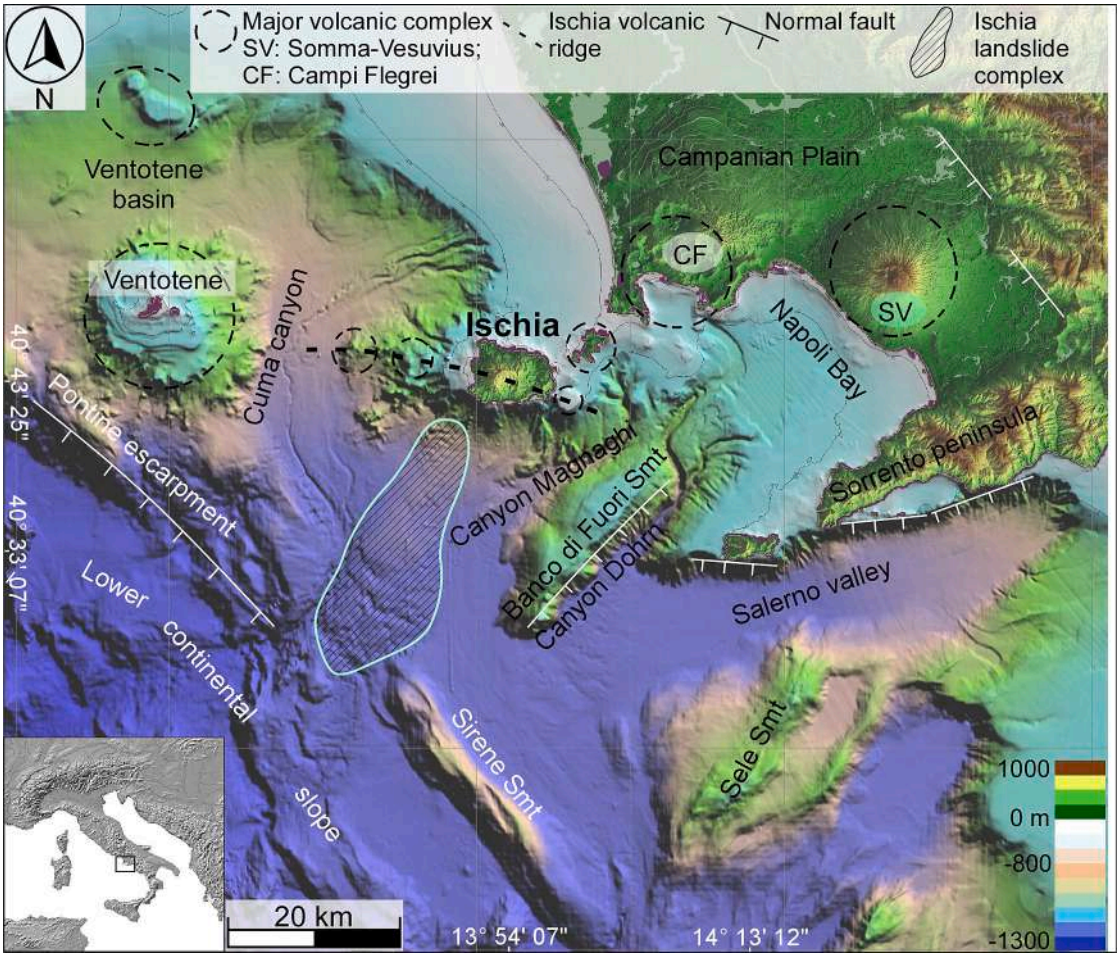

Fig. 1. Physiography and major volcanic and tectonic features of the Eastern Tyrrhenian margin off Campania region. The Ischia Landslide Complex along its southwestern slope is outlined. Shaded relief bathymetry extracted from EMODnet (European Marine Observation and Data Network).

Campania region (Fig. 1), which connects the continental mass of peninsular Italy with the back-arc domain of the Tyrrhenian Sea (Malinverno and Ryan, 1986; Conti et al., 2017). Plio-Quaternary lithospheric extension along this margin has promoted basin formation and magma ascent along regional NW-SE and secondary NE-SW trends (Acocella and Funiciello, 2006). Extension in the Campanian plain onshore and in the shelf and the slope areas off the Napoli bay has generated mostly half-graben basins according to an array of NE-SW to E-W master faults (Milia and Torrente, 1999).

Ischia Island develops in the western sector of the Bay of Naples and is part of a volcanic province that includes Campi Flegrei and Procida Island (Fig. 1). It represents the sub-aerial section of an outstanding, ca. 80 km long, E-W trending volcanic ridge, including several submerged and buried volcanic edifices (Bruno et al., 2002). The Ischia ridge separates a depositional shelf off the Campanian alluvial plain to the north from a deep basin to the south in the Bay of Naples, resulting in an unbuttressed southern flank. The upper continental slope southwest of the Island is bordered downslope by an NW-trending morphologic high, including the Sirene seamount and its northwest prolongation, aligned along a major tectonic escarpment (Marani and Gamberi, 2004), that behaves as a morphological barrier for sediments moving downslope.

The Ischia volcanic complex is the result of the coalescence of a multitude of small- to medium-scale eruptions leading to the emplacement of domes, lava flows, and pyroclastic deposits (including ignimbrites), ranging from alkali basalts to trachytes. The oldest products date to ca. 150 ka (Gillot et al., 1982) and crop out along the perimeter of the Island, especially in its southwestern and southeastern promontories (Fig. 2). The Mt. Epomeo, which dominates the central sector of the Island, consists of a partially welded tuff ("Mount Epomeo Green Tuff", MEGT, Vezzoli, 1988) related to an ignimbrite eruption occurred ca. 55 Ka. The MEGT event has been recently reconsidered as just one among other ignimbritic eruptions that occurred between 75 and 50 ka and are considered among the largest recorded on the Island (Brown et al., 2008). This ignimbritic cycle was followed by one or more caldera collapses that led to the central sector of the Island being flooded by the sea and then uplifted as a resurgent caldera dome. The uplift of Mt. Epomeo is estimated to be ca. 700–900 m and occurred between 55 ka and 5 ka, according to the latest interpretations (Sbrana et al., 2018). During the post-caldera activity, a major eruption occurred between ca. 44 and 33 ka in its western sector, whereas the activity has clustered in the eastern sector with moderate eruptions from ca. 33 ka up to historical times (Vezzoli, 1988; Orsi et al., 1991; Sbrana et al., 2018). Historical volcanic eruptions (e.g. in de Vita et al., 2010), active hydrothermal systems (e.g. in Di Napoli et al., 2011), vertical movements and seismicity (e.g. in Carlino et al., 2022) coherently indicate the presence of a degassing and still hot shallow magmatic reservoir.

During the last decades, submarine debris avalanches incorporating thousands of blocks and debris flow were documented in the Holocene sedimentary sequences along the Island's north, west and south flanks. In particular, a 1.5–3 km^3 debris avalanche (SDA in Fig. 2), due to a subaerial and/or submarine collapse, was emplaced along the steep southern flank of the Island during pre-historical (or even historical) times (Chiocci and de Alteriis, 2006; de Alteriis et al., 2010). Two similar deposits (WDA and NDA in Fig. 2) of comparable volumes assigned to pre-history were found over the shelf to the west and north of the Island (Violante et al., 2004; de Alteriis and Violante, 2009; Milia et al., 2021). Onshore, the occurrence of terrestrial or terrestrial/marine mass movements, mainly in the form of rock falls, debris flows, and debris avalanches (Della Seta et al., 2012), all spread out from Mt. Epomeo, suggest a strict connection between flank collapse and volcano-tectonic uplift. Some of these mass movements have also been favoured by the abundance of loose pyroclastic deposits over Mt. Epomeo flanks and heavy rainfalls, like the latest event in December 2022 (Romeo et al., 2023).

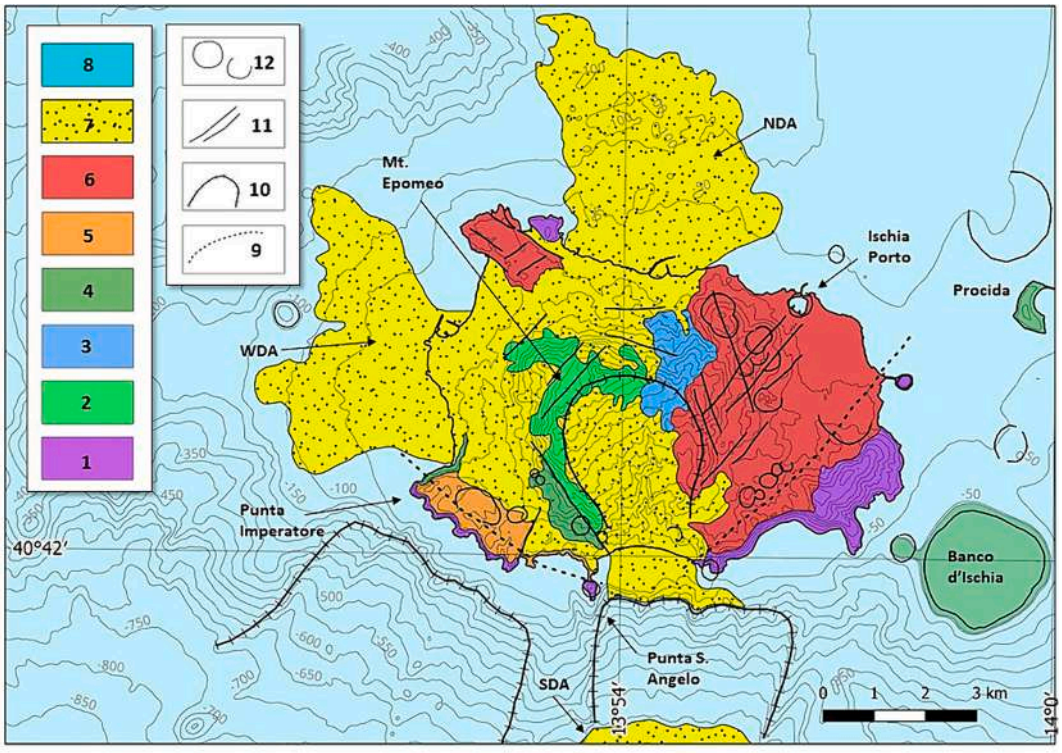

Fig. 2. Simplified volcanological map of Ischia island and part of its offshore (modified after Sbrana et al., 2018; de Alteriis and Violante, 2009). Key to map 1: ancient Ischia stage (150–73 ka) volcanics; 2: caldera-forming/ignimbritic stage (61–55 ka) volcanics; 3: post-caldera stage (61–55 ka) epiclastic and marine sediments; 4: post-caldera stage (42–45 ka) volcanics; 5: renewal volcanic activity stage (29–13 ka) volcanics; 6: recent and historical stage (10–0 ka) volcanics; 7: recent and historical stage (10–0 ka) epiclastic and mass movement deposits; 8: recent marine sediments; 9: inferred caldera rim; 10: gravity collapse scars; 11: volcano-tectonic faults; 12: volcanic centres and crater rims.

3. Marine data and methods

Swath bathymetry and high-resolution seismic reflection profiles are part of the dataset acquired onboard the Urania Research Vessel of the CNR in December 2010 within the frame of a joint project between the Istituto per l'Ambiente Marino Costiero, now Istituto Scienze Marine of Naples, of the Consiglio Nazionale delle Ricerche, Italy and the Dipartimento di Scienze della Terra e del Mare of Palermo University, Italy.

Swath bathymetric data were acquired in an area of 150 km^2 between 500 m and 1300 m depths using a hull-mounted Reson 8160 Multibeam Echosounder operating at 50 kHz. A Teledyne TSS MAHRS and a Teledyne DMS-05 were utilized for the attitude-heading dynamic motion sensor for roll and pitch corrections, respectively. Sound velocity data were acquired with a near-field probe mounted close to the echosounder transducer and along the water column (SVP soundings) every 24 h to correct acoustic beam-forming and beam-reception. The PDS2000© Thales software package acquired and processed swath bathymetric data. Data processing included: a) patch test on calibration lines, b) tide corrections, c) statistical and geometrical filters to remove coherent and incoherent noise, and d) manual removal of spikes. Processed data were gridded, generating DEMs with a cell size of 20 m. This grid was successively merged with an identical resolution grid around Ischia island acquired by IAMC-CNR (Istituto Ambiente Marino Costiero, Consiglio Nazionale delle Ricerche, Napoli, Italy) and with a lower resolution (50 m) grid for the deep-water sectors acquired by ISMAR (Istituto Scienze Marine, Consiglio Nazionale delle Ricerche Bologna, Italy) over the entire Tyrrhenian sea. The resulting bathy-morphological map was projected in UTM 33 N—Datum WGS84,

The high-resolution seismic-reflection data set consists of five dip-lines oriented NNE-SSW and five cross-lines, totalling 165 km (Fig. 3). The lines run along the toe of the Ischia island south slope in the 700–1200 m bathymetric range and cover approximately two-thirds of the investigated area. The average spacing between dip lines was slightly <1 km, while the spacing between cross lines varied from 1.2 to 2.5 km. The seismic data were acquired using a one kJoule Geo-Source Sparker acoustic source with a multi-tips (400) Sparker array and a single-channel streamer with an active section of 2.8 m. The shooting interval was 2 s, resulting in an average shot interval of 4 m. Data were recorded for 1.5 s two-way time (t.w.t) at a 10 kHz sampling rate. A DGPS system allowing 0.5 m positional accuracy was employed for navigation.

The Geo-Suite AllWorks© software package was used for seismic data processing and interpretation. Data processing included a) true amplitude recovery using a T^2 spherical divergence correction; b) band-pass (300–2000 Hz) "Finite impulse response" filter using a filter length of 256 samples; c) swell-filter; d) trace mixing of three traces for the enhancement of the horizontal signal; e) time-variant gain to boost amplitudes of deeper arrivals; f) mutes to eliminate the noise on the water column. Signal penetration was found to exceed 300 ms t.w.t. The vertical resolution was up to 0.5 m in the near sub-seafloor.

Time-to-depth conversion was performed using 1500 and 1800 m/s velocities for the water column and subsurface sediments. Depth-converted sections were plotted with a vertical exaggeration of 10× to enhance the geometry of stratal patterns and thus assist seismic interpretation.

Two 6-m long gravity sediment cores, 9 cm in diameter, provided shallow sub-bottom ground-truthing at two sites inside the investigated area at 960 m and 1100 m below sea level (bsl hereafter). Cores were split into two halves, photographed and described for lithology, texture and grain fabric. A core repository belonging to the ISMAR-Naples complements this new dataset.

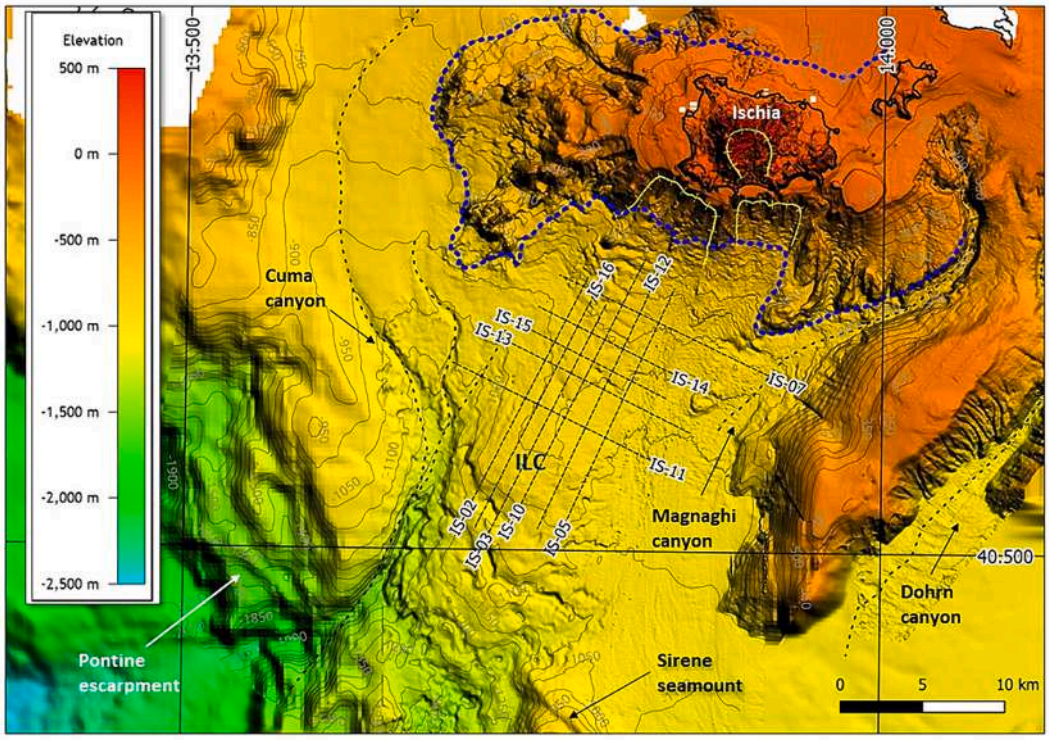

Fig. 3. Shaded-relief bathymetry resulting from the merge and processing of the 2010 survey multibeam survey with previous surveys carried out in the Ischia island offshore in the past 20 years; the DTM has a grid cell size from 20 to 1000 m isobaths and 50 m for greater depths. Main morphologic features are outlined; ILC: Ischia Landslide Complex; dashed black lines are canyon axes; the blue dashed line is the limit of Ischia volcanic ridge; yellow lines are gravity collapse scars; tracks and labels of the seismic profiles used for this study are reported. Discussion in the text. (For interpretation of the references to colour in this figure legend, the reader is referred to the web version of this article.)

4. Results

4.1. Seafloor morphology

The investigated area extends from the Island southern offshore to the upper continental slope limited to the southwest by the Sirene Seamount and the Pontine escarpment down to approximately 1500 m depth. The analysis of multibeam bathymetry shows, at first sight, an overall N-S asymmetry of the Ischia volcanic ridge, with the southern and southwestern flanks deeper and steeper than the others. South and southwest of the Island, the deep indentation of the bathymetric contour suggests that a large sector of the submerged volcanic edifice is missing (dashed blue line in Fig. 3). Here, the shelf is only 0.7–1 km wide while the shelf break is at 60–70 m bsl. The latter values are significantly lower than the western and northern offshore shelf break depths, about 120–170 m bsl. The southern shelf-break is engraved by gullies, small canyon heads and two collapse scars: the first is located off the southwestern promontory of the Island, while the second correlates to the previously mentioned SDA located off the southern coast (Fig. 3).

The newly multibeam data reveals a long tongue of deformed and locally counter-sloping seafloor, elongated from NNE to SSW, hereafter Ischia Landslide Complex (ILC). ILC extends along the slope from 850 m bsl until up to 40 km from the Island's coast; it barely exceeds 12 km in width over an area of 330 km^2. Its distal lobe attains 1400 m bsl after passing through the already mentioned 12–14 km wide breach along the Pontine escarpment between the Sirene seamount and its prolongation (Fig. 3).

Morphometric analysis, based on slope gradient map and bathymetric profiles (Figs. 4 and 5), has allowed the recognition of three main morphologic domains inside ILC: the upper-slope, the bulge-slope and the distal toe-section. The upper-slope domain is characterized by the remnant of a collapse scar, 5.2 km wide, that engraves the Island's southwestern flank and its shelf from 70 to 500 m bsl. The mean slope gradient in this section is 18° with maximum values of 35°, attaining higher values in correspondence to near vertical walls inside the collapse scar. More downslope, between 600 m and 900 m bsl, a series of elongated, slope-parallel undulations, with amplitudes of 25–30 m and wavelengths between 0.3 and 1 km, are identified over an area of about 50 km^2 with a slope gradient varying from 3° and 1°.

In the bulge-slope domain, the mean gradient significantly decreases to <1°, from 900 to 1000 m bsl. In this section, a low-relief outer bulge gently rises from the seafloor, culminating at about 20 km from the island shore. It has a topographic expression of about 15 m and 50 m along and across dip, respectively. In this section, the bulge is partly eroded by the Cuma Canyon along its western flank, while its eastern flank is almost flat with an average slope gradient of <1°. The ILC is partially contiguous with the Ischia SDA, characterized by hummocky topography due to the blocks placed during the avalanche. A flat-floor depression, about 4 km wide, lies immediately upslope of the bulge summit at about 950 m bsl.

The distal toe section extends from 1000 to 1400 m bsl. A tongue-shaped lobe with rough topography due to discontinuous and arcuate scarps and irregularly spaced, elongated knobs, depressions and ridges characterizes it. Here, slope gradients can exceed 15° in correspondence to these morphological features. This section corresponds to the frontal lobe of the slump that gently flows across the breach of the Pontine escarpment.

4.2. Seismic stratigraphy

The sedimentary multilayer corresponding to the southern apron of the Ischia volcanic edifice consists of hemipelagic sediments alternating with volcano-clastic materials or solid volcanic rocks. The relative abundance of the latter moving from the distal area to the Island flanks significantly reduces the acoustic penetration and, thus, the possibility of fully imaging the upslope sections of the apron.

The internal geometry of the apron is based on the interpretation of the seismic grid, which is made of five dip-lines and five cross-lines that

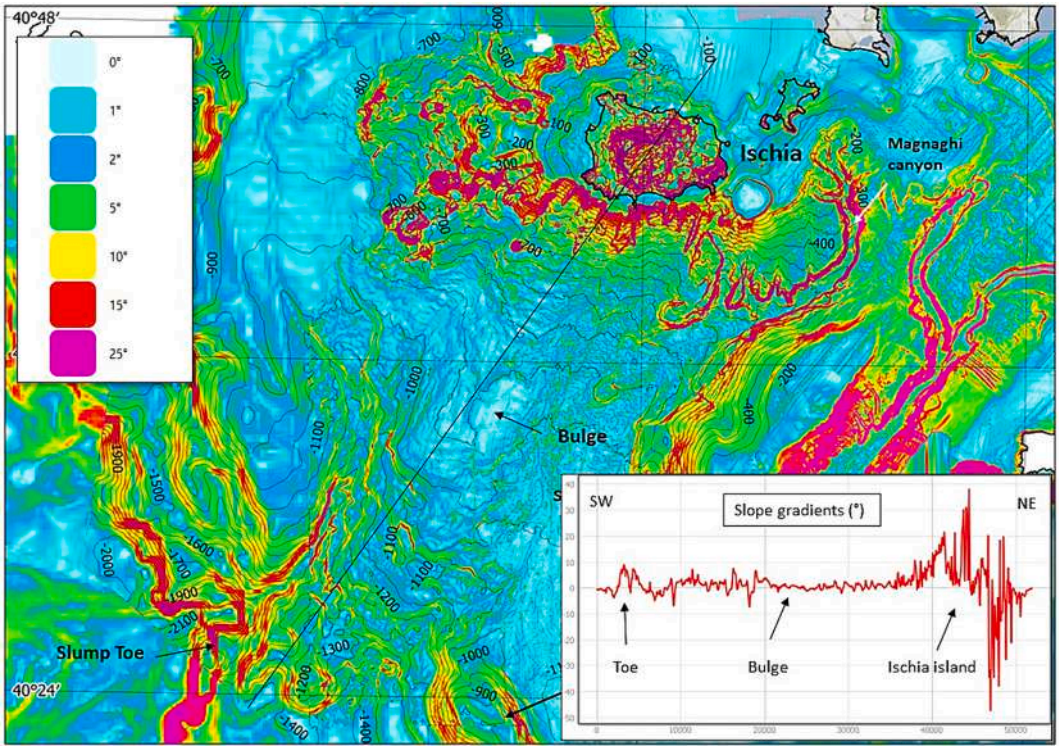

Fig. 4. Slope gradient map (degrees from horizontal) derived from the previous DTM and slope gradients (inset) along the SW-NE profile crossing ILC and the Island (thin black line). Note gradients >25° all along the scalloped submarine flank south of the Ischia volcanic ridge and in the ILC toe region; gradients <2° in the 800–1000 m depths bulge section. Discussion in the text.

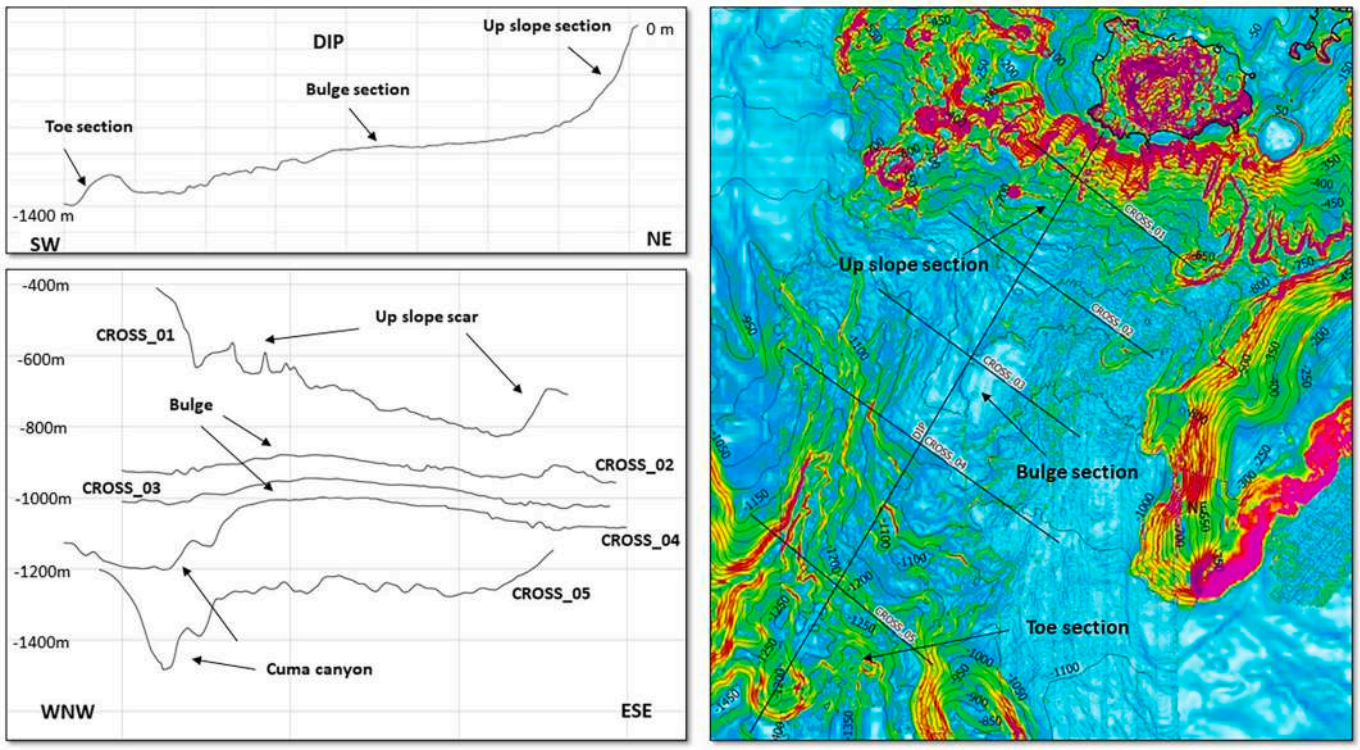

Fig. 5. Transverse and longitudinal bathymetric profiles across ILC. Note the concave profile in the erosional, upslope section evolving to convex shapes in the bulge area limited to the west by the Cuma Canyon. Discussion in the text.

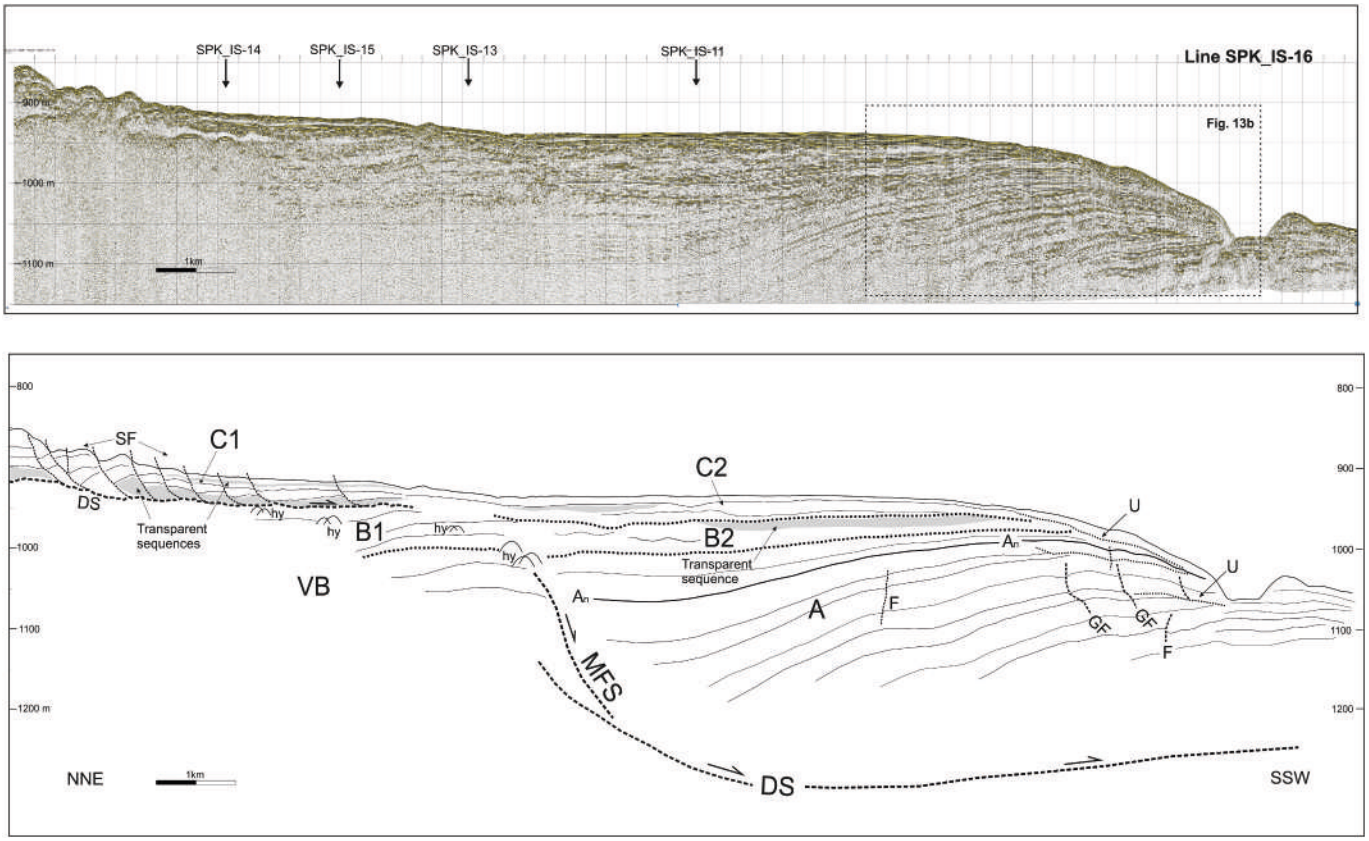

Fig. 6. Dip sparker seismic line SPK_IS_16 along the western side of ILC and interpretation. MFS: main slump failure surface; DS: detachment surface; SF: shallow slumps failure surfaces; GF: failure surface; U: local unconformities; A, B1, B2, C1, C2: Seismic units; An: reflector near the top of unit A. Discussion in the text. Location in Fig. 3.

cross it. Four seismo-stratigraphic units, each characterized by similar acoustic facies and stratal geometry, limited by unconformities or by planar detachment or concave (listric) surfaces, have been recognized inside the sedimentary multilayer (in the following description, refer to seismic profiles in Figs. 6, 7, 8, 9, 10 and 11).

Unit V.B. shows a succession of highly discontinuous, moderate- to high-amplitude reflectors, locally alternating with acoustically opaque, reflection-free zones. Unit V.B. is interpreted as the volcanic basement or, more likely, that part of the apron with a significant prevalence of volcanoclastic material and volcanic rocks.

Unit A is characterized by a rhythmic succession of continuous, mid to high-amplitude reflections and transparent intervals, all arranged in a broad anticline with landwards divergent stratal patterns. In the outermost sector of unit A, local unconformities and high and low-angle growth faults can be recognized (U and GF in Figs. 6–10). Unit A has a maximum measured thickness of at least 300 m based on what is visible on seismics.

Unit B unconformably overlies units V.B. and A. It extends with different seismic characters from the toe of the volcanic edifice until the outer bulge crest. The upper section of unit B (B1 in the figures) shows moderate- to very low-amplitude, discontinuous and subparallel to undulated reflectors. The lower section (B2 in the Figures) is seismically characterized by well-stratified, high-amplitude reflectors interbedded with semi-transparent and low-amplitude reflectors. Chaotic to transparent reflections significantly increase from west to east inside the ILC. On lines IS-10 and IS-12, the B2 Unit becomes fully transparent apart from isolated reflections and hyperbolas and attains its maximum thickness as a wedge-shaped basin.

Unit C, the most recent seismic unit, is characterized by laterally continuous, medium to high-amplitude reflectors alternating with transparent intervals. It includes an upslope and a downslope section (respectively C1 and C2 in Figs. 6–10). Incipient slumpings caused by slump surfaces soling out on a slope-parallel detachment surface (DS in Figs. 6–10) characterize the upslope section of C1. Unit C1 gets thicker upslope, passing from about 40 m to 90 m. The downslope section C2 is generally thinner and does not show evidence of deformation. It consists of planar parallel stratal patterns and transparent intervals. It unconformably rests above the B2 sequence.

4.3. Architecture of the Ischia Landslide complex

Based on the previously described seismic units, the internal architecture of the ILC can be described as the ensemble of three members genetically connected between them: 1) a basal slump anticline (BSA), 2) a mid-mass-movement complex (MMC), and 3) an upper mass-movement complex (UMC). As for the above, refer to seismic profiles in Figs. 6, 7, 8, 9, 10 and 11 with details in Figs. 12 and 13.

4.3.1. The basal slump anticline – BSA (Seismic Unit a)

All seaward dipping-oriented seismic lines show asymmetric antiform, consisting of a main body and a toe area (Figs. 6, 7, 8 and 9). Landward dipping reflectors characterize the proximal sector of the BSA while the entire geometry of the slump toe can be observed on bathymetry (Fig. 5). The dip of dipping strata decreases from 9° (eastern sector: Lines IS-10 and IS-12 in Figs. 8 and 9) to 4°-5° (western sector: Lines IS-16 and IS-03 in Figs. 6 and 7) while lower values occur on the toe area. Overall, the sediment thickness involved in the deformation is at least 300 m.

In plain view, the internal geometry of BSA was reconstructed based on the picking of the reflector A_n identified in seismic profiles close to

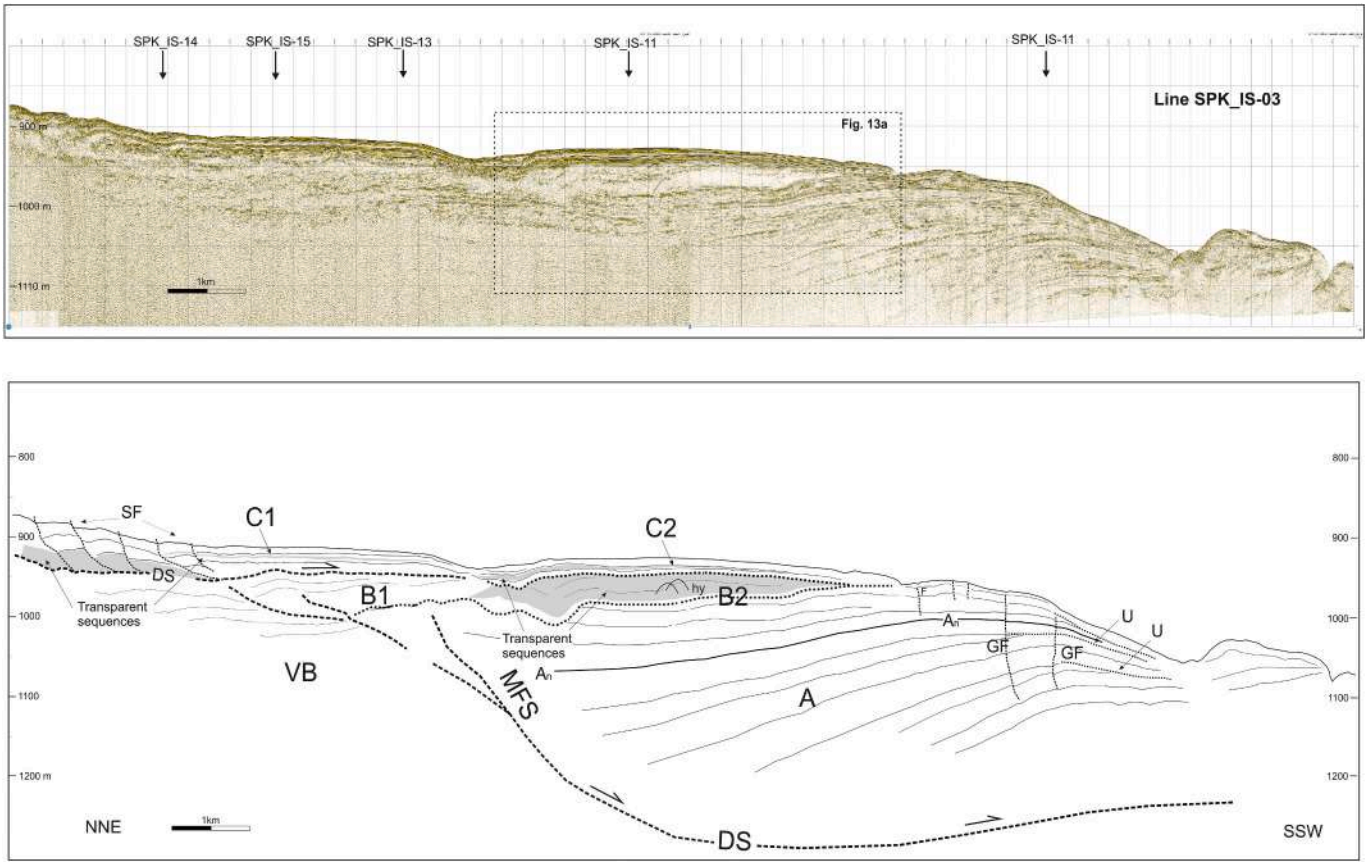

Fig. 7. Dip sparker seismic line SPK_IS_03 along the western side of ILC and interpretation. MFS: main slump failure surface; DS: detachment surface; SF: shallow slumps failure surfaces; GF: failure surface; U: local unconformities; A, B1, B2, C1, C2: Seismic units; An: reflector near the top of unit A. Discussion in the text. Location in Fig. 3.

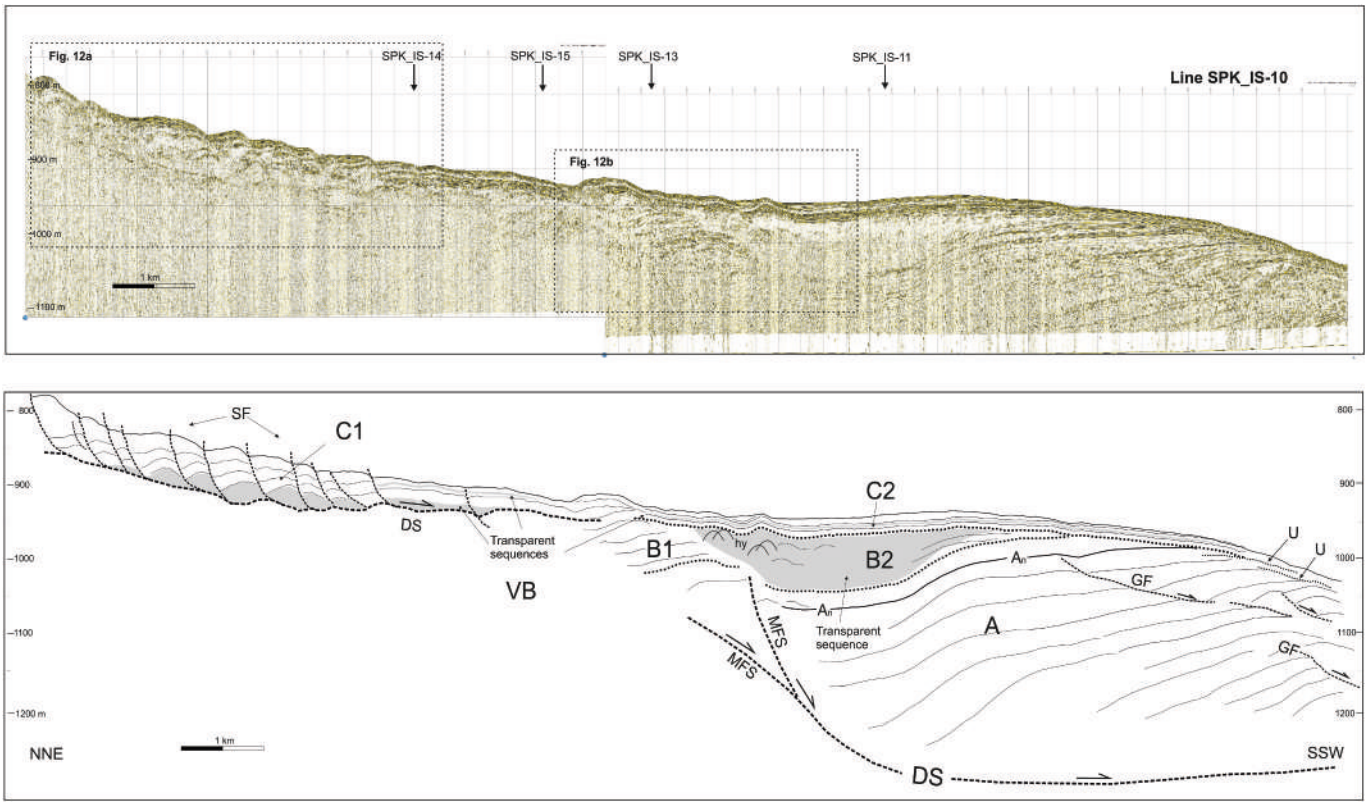

Fig. 8. Dip sparker seismic line SPK_IS_10 along the eastern side of ILC and interpretation. MFS: main slump failure surface; DS: detachment surface; SF: shallow slumps failure surfaces; GF: failure surface; U: local unconformities; A, B1, B2, C1, C2: Seismic units; An: reflector near the top of unit A. Discussion in the text. Location in Fig. 3.

the top of the antiform. The contour map of such a reflector shows a non-cylindrical, asymmetric fold on turn consisting of two secondary crest folds (Fig. 14a). The fold wavelength is about 8 km along dip (NNE-SSW direction) and between 2 and 3 km across dip (WNW-ESE direction) for each of the two secondary folds with an average amplitude of about 150 m. On the dip seismic lines, it can be seen that the fold crest slightly migrates upslope of about 2 km inside BSA, confirming the asymmetry and the not-vertical fold axis. Seaward, the BSA is affected by low-angle *syn*-sedimentary failure surfaces, i.e. growth faults and local unconformities that truncate stratal patterns (Fig. 13).

The seismic characters of unit A (see previous section) suggest that most of this structure is composed of well-layered hemipelagite interbedded with turbidites and occasionally with thicker (even in the order of one or more metre) mass transport deposit (e.g., slumping, debris flows) characterized by transparent seismic facies. Based on the internal stratal geometry and morphologic features, the BSA is interpreted as the extensional domain of a large-scale, syn-depositional, non-cylindrical and laterally confined fold formed by slumping. The seismic data interpretation confirms the relationships between the subsurface extension of BSA and the morphological bulge observed on bathymetry. (Fig. 14a). A conservative estimate of the volume of BSA, based on an areal extension of 190 km^2 (including the toe section) and an average thickness of 200 m above the basal detachment (see following sections) results in about 40 Km^3.

4.3.2. The mid-mass-movement complex - MMC (Seismic Units B1 and B2)

A volcano-sedimentary sequence (MMC hereafter) corresponding to seismic Units B1 and B2 overlies BSA. The proximal section of MMC (Seismic Unit B1), which is located upslope of the mentioned flat floor depression, consists of undulated, locally faulted layers (Fig. 12b). The distal section of MMC appears, on the contrary, as a wedge-shaped, seismically chaotic to transparent body which only locally retains stratal patterns (Seismic Unit B2). It attains a maximum thickness of about 100 m (Figs. 12b and 13a) that fills the "half-graben" basin formed in the internal sector of BSA. Its chaotic to fully transparent seismic facies suggest a relatively fast mass movement consisting of debris flows and/or debris avalanches with a high content of clay matrix that rapidly filled the accommodation space in the internal sector of BSA after the deformational phase.

4.3.3. The upslope-mass-movement complex - UMC (Seismic Units C1 and C2)

The upper slope section of UMC (Seismic Unit C1) consists of a volcano-sedimentary sequence thickening towards the toe of the Ischia edifice. Here UMC shows evidence of incipient slumping controlled by sets of sliding surfaces (with concave, listric geometry), spaced on average 200–300 m, that confine packets of folded or landward-tilted reflectors (Fig. 12a). These structures correspond to the previously described seafloor undulations (creep) imaged by swath bathymetry in the proximal segment of the ILC (Figs. 5). These listric, sliding surfaces sole out over a slope-parallel detachment, $<2^{\circ}$ steep, located at a depth ranging from 60 to 70 m below seafloor. The detachment mainly occurs along seismically transparent sequences, suggesting possible debris flow intervals with high clay fraction. Downslope, UMC appears as a sub-horizontal sedimentary body (Seismic Unit C2), not involved in the slumping that fills the flat floor depression.

UMC is the only member that cores have sampled. Analysis of cores C-001 and C-002, respectively, in the flat floor depression and the toe region (Fig. 14a and b), indicates layered hemipelagites with interbedded volcanoclastic debris flows and turbidites. Notably, core C-01 has recovered debris flow between 0.5 m and 1 m sub-bottom depth which correlates to the Ischia SDA of pre-historical age (de Alteriis et al., 2010). Overall, UMC is interpreted as being a sequence of deposits resulting from intermittent debris flow and turbidite events sourced

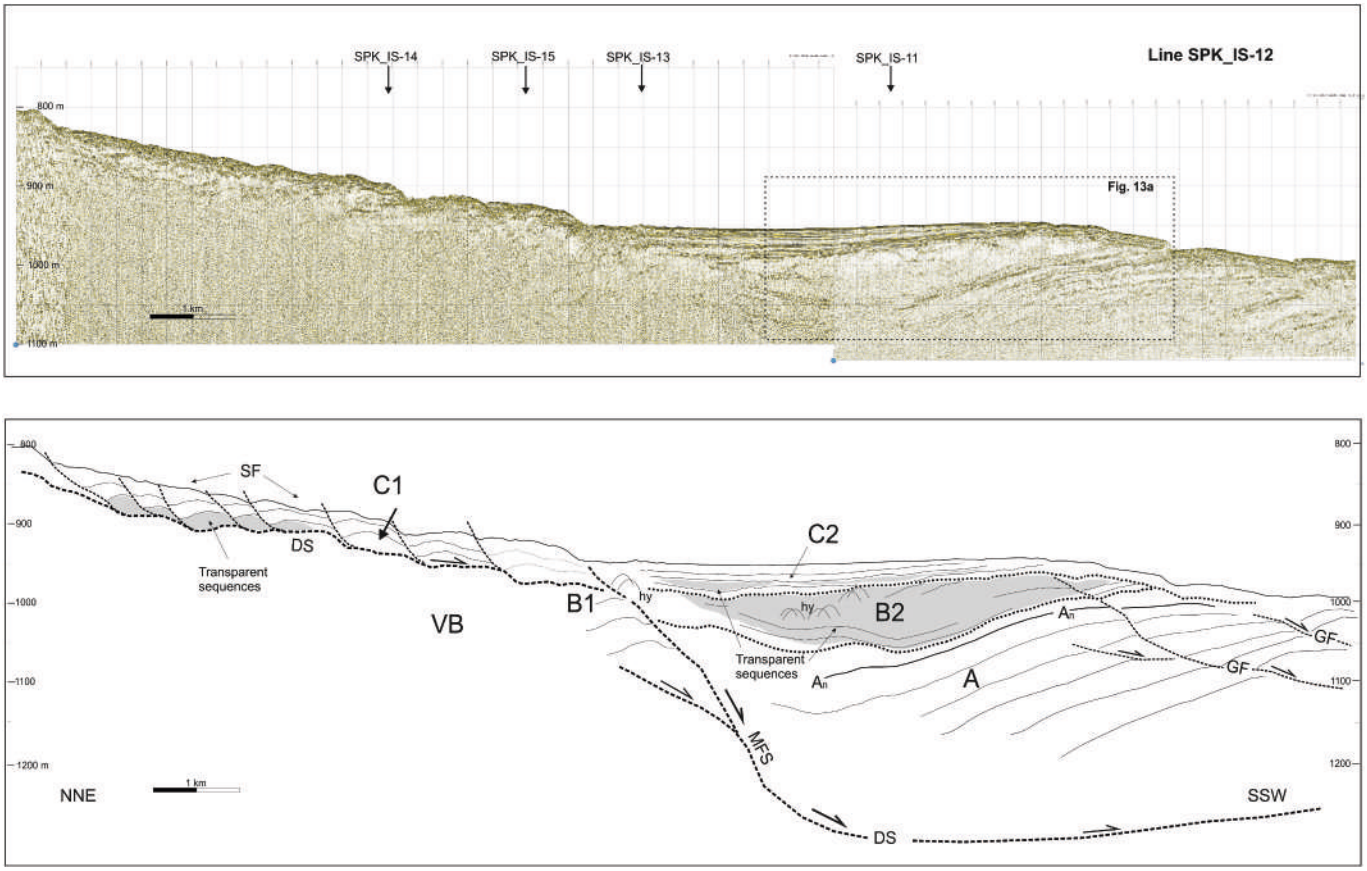

Fig. 9. Dip sparker seismic line SPK_IS_12 along the eastern side of ILC and interpretation. MFS: main slump failure surface; DS: detachment surface; SF: shallow slumps failure surfaces; GF: failure surface; U: local unconformities; A, B1, B2, C1, C2: Seismic units; An: reflector near the top of unit A. Discussion in the text. Location in Fig. 3.

from the Ischia volcanic edifice, alternated with hemipelagic deposition. Based on an areal extension of 155 km^2 and an average thickness of 30 m, the upslope UMC section volume estimate is about 5 Km^3.

5. Discussion

The data we present show that a sector of the southern volcano-sedimentary apron off Ischia Island has undergone a large-scale failure with different types of mass movements that are, in our model, genetically connected between them (Fig. 15a). These are 1) a basal slump (BSA) stage characterized by *syn*-kinematic deposition, 2) a chiefly turbiditic/debris flows stage (MMC) filling the accommodation space formed in the internal sector of the BSA at the end of the deformation stage and 3) a shallow detachment stage (UMC) in the upper slope section. The divergent stratal pattern of reflections inside BSA and syn-sedimentary failure surfaces that dissect the upper section of UMC suggests that failure occurred at a slow strain rate for both mass movements. On the contrary, the overall transparent or chaotic seismic facies with minimal preservation of the original layering inside MMC suggest that it was emplaced as a fast, disintegrative process. The causal relationship between the origin of the BSA and the subsequent evolution of the entire slope stresses the importance of understanding its extent, timing, and possible factors promoting failure.

5.1. Depth of basal detachment and timing of the deformation

The BSA internal geometry requires a main base failure surface (MFS in all figures) that soles out over detachment at its base. However, such detachment cannot be observed on seismic data and can only be inferred using geometric constraints. The depth of the detachment formed at the base of the BSA can be calculated in analogy to what happens for roll-over anticlines (Dula, 1991) in extensional tectonics. However, it is worth recalling that the term slump in its broader sense, i.e., "a mass moving on an upwards-concave surface with relevant internal deformation" (e.g. Mulder and Cochonat, 1996), does not contradict the conceptual model of extensional rollovers although the two processes (gravity vs tectonics) significantly differ with regard to the space-time scale. Thus, in our interpretation, the wedge-shaped internal sector of the anticline corresponds to a *syn*-sedimentary wedge in the hanging wall controlled by a main failure surface (or normal fault in structural terminology) with listric geometry (MFS in all figures) that soles out over a flat detachment at depth. The detachment depth (z) for listric faults can be inferred by using different methods based on the basin (cross-section) area (A) dropped below the regional level and the heave (h) or the displacement (d) (Fig. 15a) across the fault according to the following simple relationship (Poblet and Bulnes, 2005):

$$z = A/h \text{ or } z = A/d.$$

Although it is difficult to define a clear pre-deformation horizon due to the strongly syn-depositional character of the mass-transport process, the heave across the fault and the basin dropped below the regional level can be assessed at first approximation. Based on this approach, we have estimated a heave variable from 800 to 1000 m and a cross-section area of the dropped basin of 360 × 10^3 m^2. This leads to detachment depths that vary from 350 to 450 m below the regional level, depending on the adopted parameters. It must be remarked that this method assumes a 2D geometry that is not the case for our slump, whose basal detachment is concave in cross-section (Fig. 11). Therefore, the 350–450 m detachment depth must be considered as the maximum depth attained along the central axis of the slump. Fault geometries inside BSA suggest that it

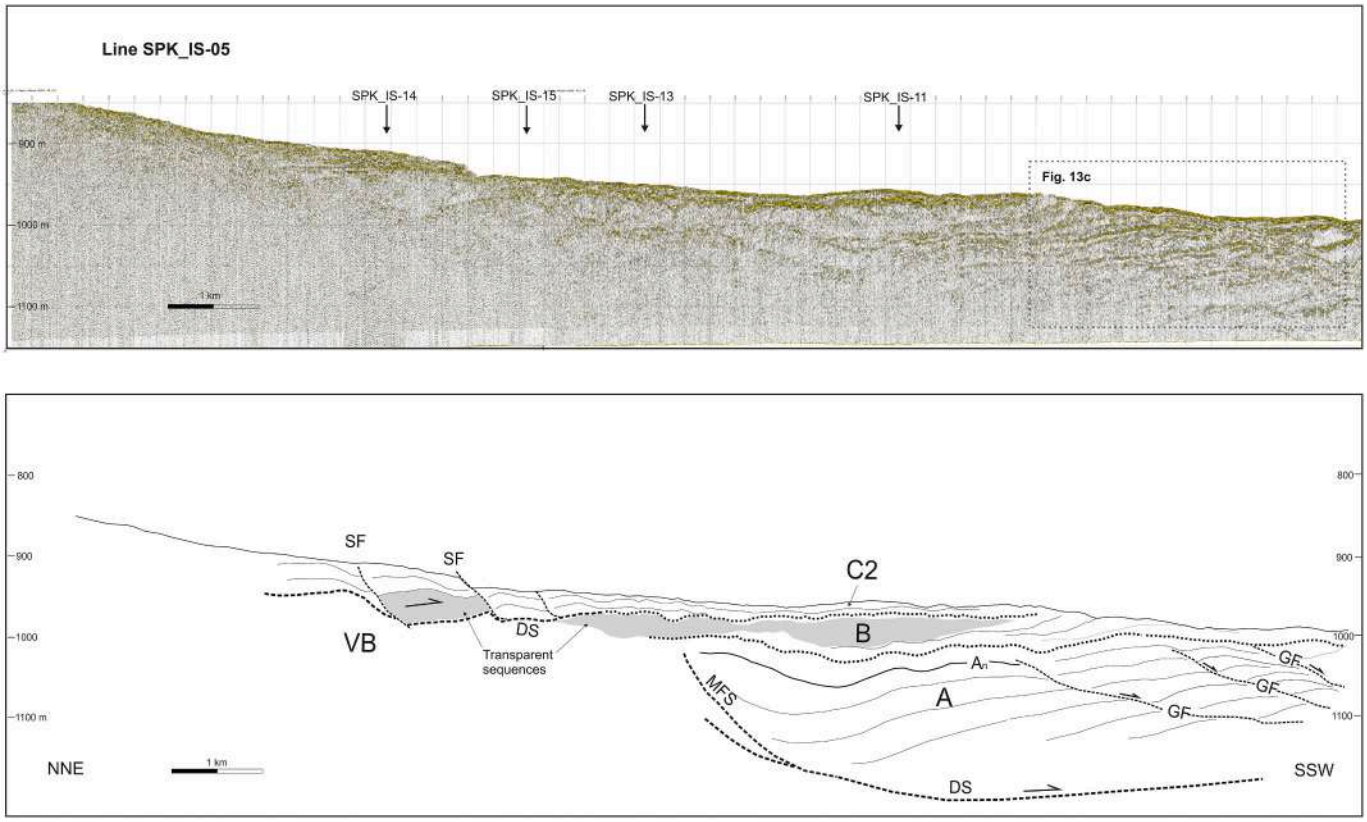

Fig. 10. Dip sparker seismic line SPK_IS_05 along the eastern side of ILC and interpretation. MFS: main slump failure surface; DS: detachment surface; SF: shallow slumps failure surfaces; GF: failure surface; U: local unconformities; A, B1, B2, C1, C2: Seismic units; An: reflector near the top of unit A. Discussion in the text. Location in Fig. 3.

represents the extensional domain of a relatively deep-seated slump whose toe is further downslope. First-order evidence that supports an extensional, gravity-driven stress field inside BSA are a) the absence of reverse faults or thrust planes; b) the divergent (fanned) stratal geometry of Unit A deposits, which is characteristic of thin-skinned, gravity-driven deformation in sequences of poorly lithified sediment; c) the occurrence of incipient low-angle *syn*-sedimentary failure surfaces (or growth-faults) in the distal sector of the main body. At the same time, the absence of any morphological or seismo-stratigraphic evidence of extensional faults outside the lobe allows for the ruling out any regional tectonic component. Therefore, this interpretation allows us to rule out alternative views that consider the basal fold as a ramp or thrust anticline in analogy to a wide range of similar structures observed at the toe of submarine slumps (e.g. Storegga slide, Færseth and Sætersmoen, 2008; Frey-Martinez et al., 2005) or in deep water thrusting (e.g. Niger delta, Corredor et al., 2005).

Regarding the timing of the deformation process, the onset and duration of the deformation responsible for ILC are challenging to assess. This is due to its syn-sedimentary character, the lack of clear post-deformational sequences and several morphological evidences suggesting that the landslide complex is still moving. We can only tentatively assess the ending time of the main deformational phase based on the thickness of the undeformed UMC member (i.e. C2 seismic unit) that seals MMC and BSA and on the available sedimentary rates in the region.

C2 has a maximum thickness of 30 m and includes hemipelagites, turbidite layers and debris flow deposits. Such thickness does not consider stratigraphic gaps due to subsequent erosion or low-angle sedimentary failures and, therefore, would lead to an age underestimate. At the same time, the non-hemipelagic fraction (turbidites and debris flow) inside the burial tends to increase the age estimate since it includes geologically instantaneous deposits. Therefore, in the first approximation, we can assume that the two effects compensate for each other.

By considering a 70% hemipelagic fraction over a thickness of 30 m for C2, we obtain about 20 m of the true sedimentary record. In the area, an average sedimentation rate ranging between 0.25 and 0.45 m/kyr has been measured from nearby gravity cores (CS-011, TC-055, C-848, C-1108, C-1107 in Fig. 14a) (de Alteriis et al., 2010). Thus, by using 0.25–0.45 m/kyr sedimentary rates and a 20 m burial depth, we obtain an age range of 80–45 ka for the end of the main deformational phase. Thus, the slump's main acceleration phase most likely started in the Mid-Late Pleistocene and ended or was partly coeval with the 75–33 ka time interval characterized by the most voluminous and energetic eruptions that occurred on the Island (Brown et al., 2008) among which that of Mount Epomeo Green Tuff at 55 ka (Gillot et al., 1982; Vezzoli, 1988). The causal correlation between the ignimbritic cycle and deep-seated flank instability is only a working hypothesis at the current state of knowledge. Finally, a wide range of morphological (upslope creep, irregular topography at the slump toe) and seismic evidence (shallow seated slump, strata deformation, syn-sedimentary failures) suggest that the deformation of the ILC is still active.

5.2. *Factors promoting failure*

In this section, we investigate the implications of our results on the factors promoting the failure of the Ischia Landslide Complex (ILC) and its kinematics.

Our data show that different sectors of the volcano-sedimentary apron off Ischia Island have undergone a large-scale failure with different but closely interrelated landsliding mechanisms. It is worth

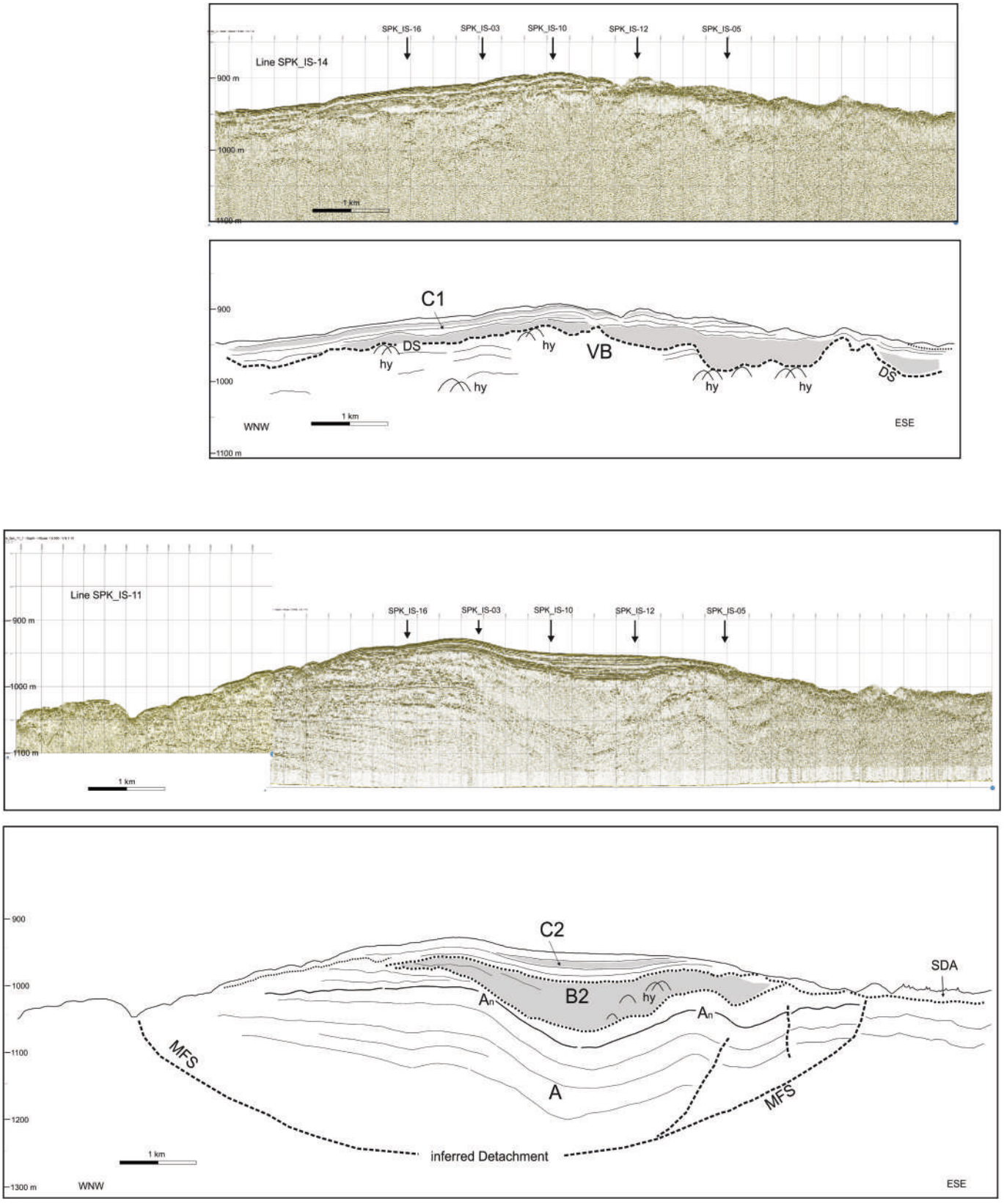

Fig. 11. Cross sparker seismic lines SPK_IS_14 and SPK_IS_11 across the up-slope (upper figure) and downslope sections of ILC. MFS: main slump failure surface; VB, A, B2, C1, C2: Seismic units; An: reflector near the top of unit A; SDA: Ischia southern debris avalanche.

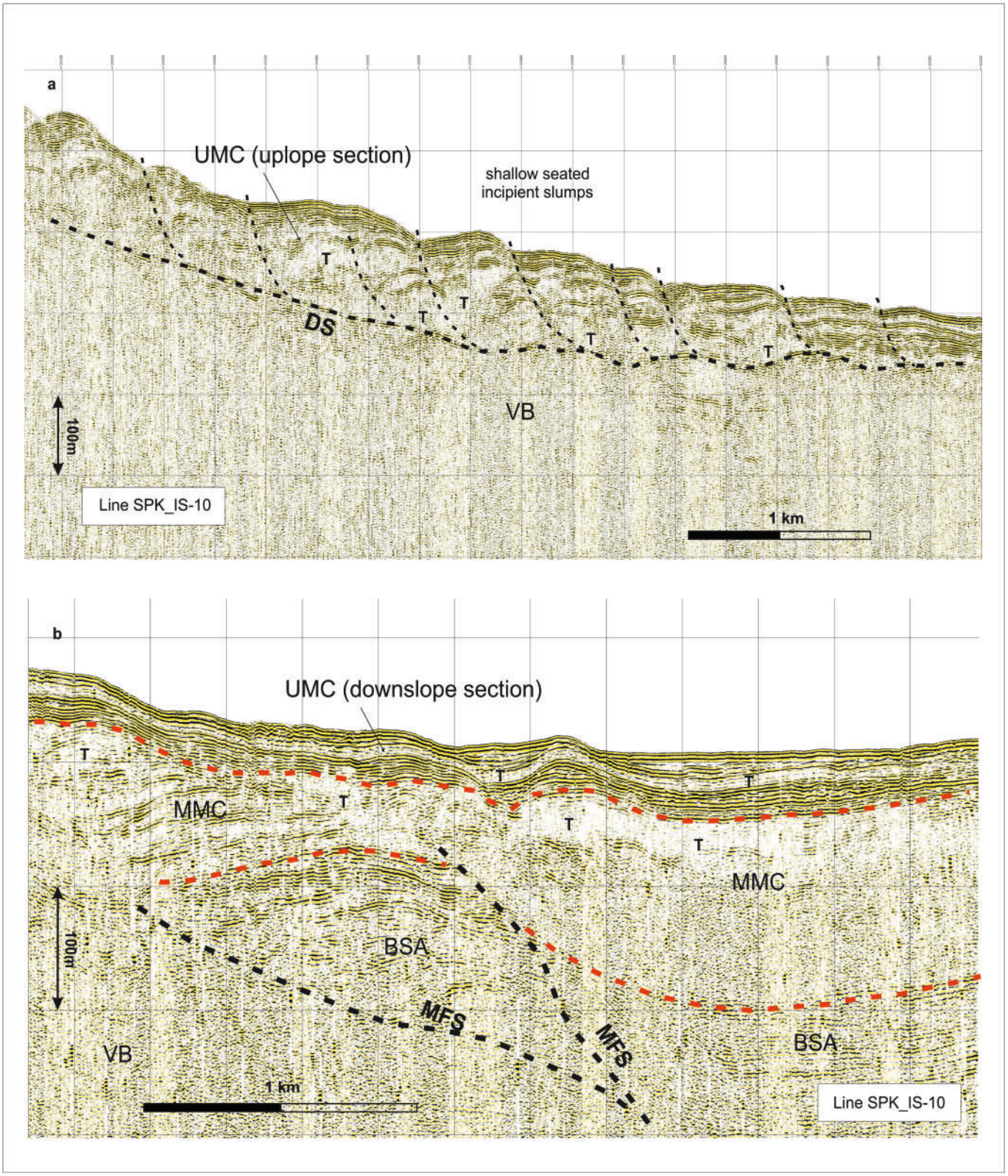

Fig. 12. Details of seismic profile IS-10; a) note upper slope slumps affecting UMC; b): note stratal deformation at the termination of the main failure surface MFS; BSA: Basal Slump Anticline; MMC: Mid Mass-Movement complex; VB: volcanic basement; DS: detachment surface; T: transparent seismic facies. Dashed red lines are unconformities limiting main sequences. Discussion in the text. The entire profile is in Fig. 8. (For interpretation of the references to colour in this figure legend, the reader is referred to the web version of this article.)

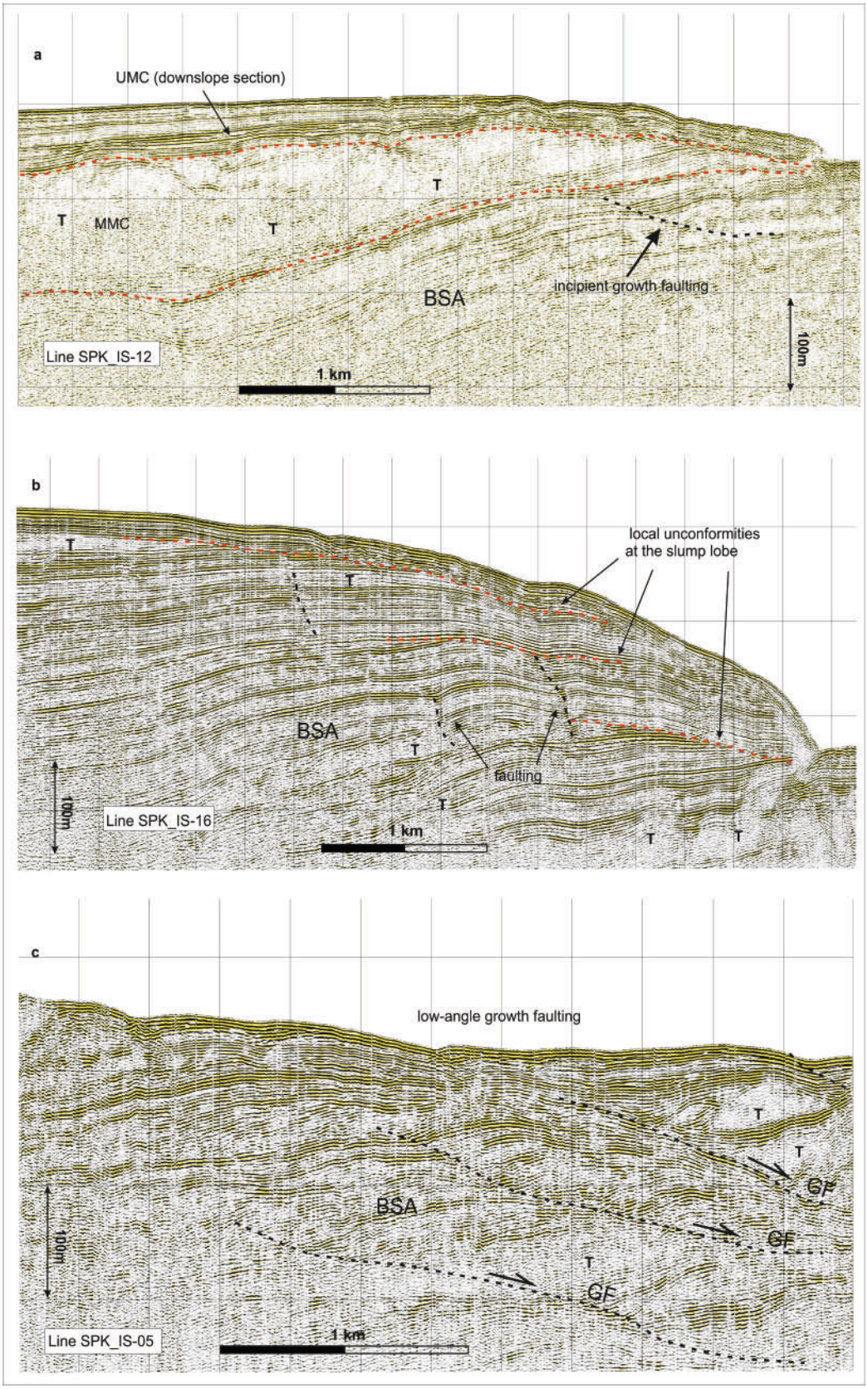

Fig. 13. Details of seismic profiles IS-12, IS-16 and IS-05; a). transparent to chaotic filling on the backlimb of BSA; b): details of the frontal lobe of BSA with near vertical faults and local unconformities; c): details of low-angle growth faults on the BSA forelimb. BSA: Basal Slump Anticline; MMC: Mid Mass-Movement complex; VB: volcanic basement; DS: detachment surface; T: transparent seismic facies. Dashed red lines are unconformities limiting main sequences. Discussion in the text. Entire profiles in Figs. 6, 9 and 10. (For interpretation of the references to colour in this figure legend, the reader is referred to the web version of this article.)

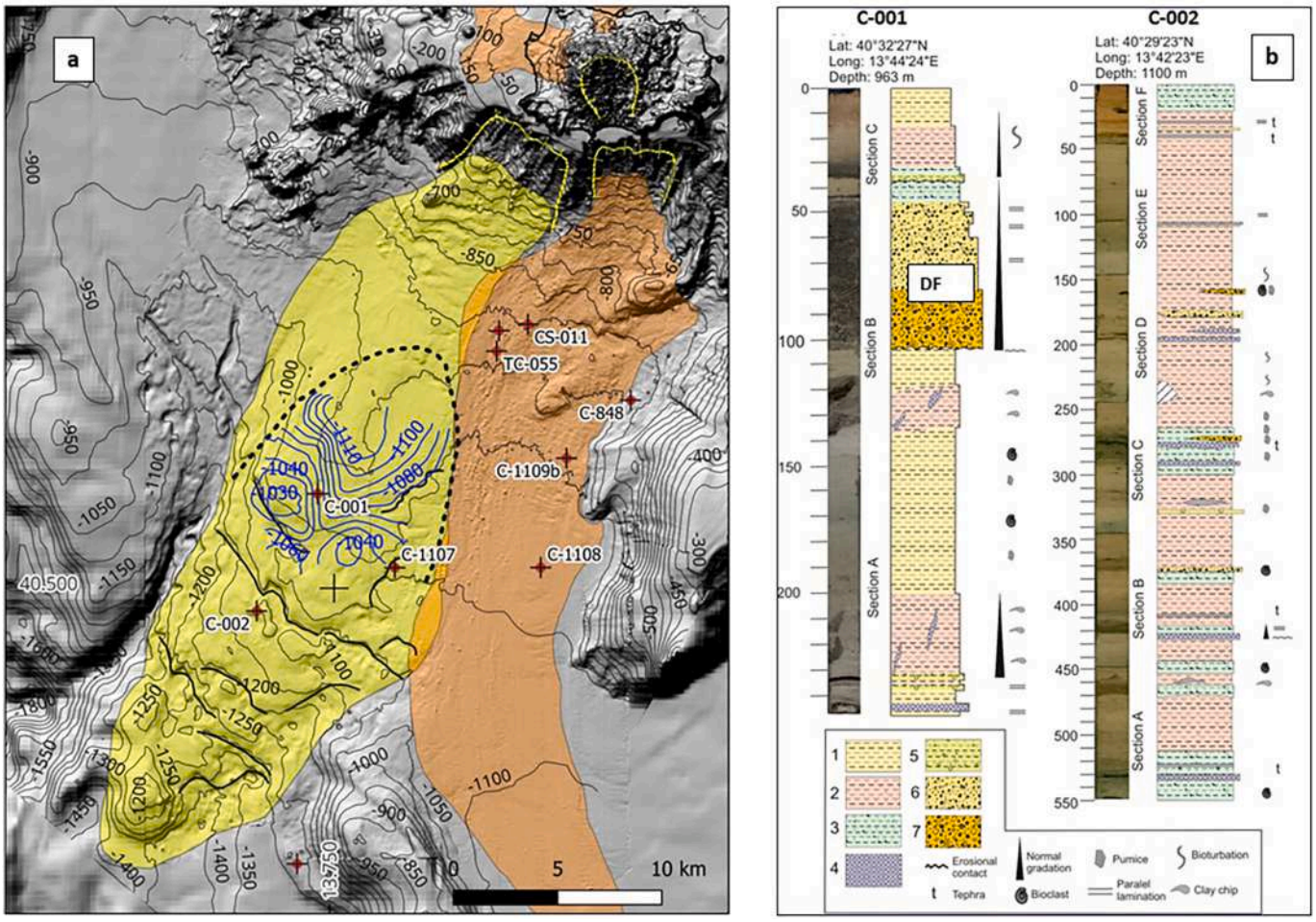

Fig. 14. a) Map of the extent of ILC (yellow) and debris avalanches (orange) with main features recognized from morphology and seismo-stratigraphy. Blue contour lines are the depth (m) to the top of BSA, the thin black contour is bathymetry, dashed thick black line is the main failure surface (MFS) in plan view. Locations of C-001 and C-002 cores acquired during the 2010 cruise and from previous surveys (de Alteriis et al., 2010) are reported. b) Composite log of cores C-001 and C-002. Legend: 1, 2 and 3: Hemipelagic, clayey silts or silty clays; 4: Fine sand levels (possibly turbiditic); 5: Airfall tephra (pumice, scoriae, lithics); 6 and 7: Volcanoclastic debris flow (coarse pumices, lithics) with variable clay matrix; DF is the debris flow associated to Ischia southern debris avalanche (SDA).(For interpretation of the references to color in this figure legend, the reader is referred to the web version of this article.)

noting that incipient creep and slumping on the upper slope have not been observed over the other flanks of the volcanic edifice but occur only in correspondence to the BSA. This evidence further supports the genetic correlation between the deep-seated BSA downslope and the shallow-seated slumps upslope. The possible causative factors that have promoted failure can be included in the following two main categories:

5.2.1. Failure of the continental slope unrelated to the dynamics of the Ischia volcanic edifice

It has been observed that submarine landslides do not appear to be significantly influenced by slope gradients (Hühnerbach et al., 2004) but rather by certain predisposing factors, including the presence of a basal low-friction layer coupled with a trigger factor, e.g. earthquakes and sea-level changes. The ILC is an outstanding event with a volume (conservative) appraisal of 40–50 km^3. Its origin as a typical submarine landslide unrelated to Ischia volcano cannot be ruled out but, in our reasoning, seems quite improbable. Analogue examples of comparable-size landslides not related to volcanisms along the entire Eastern Tyrrhenian margin are lacking even though several sectors of this margin have been recently explored in the frame of regional-scale projects aimed at geo-hazard evaluation (i.e. MaGIC, Chiocci et al., 2021). Apart from many translational slides with volumes in the range of 0.1–2 km^3 recognized in the shelf break/slope region (for instance, Budillon et al., 2014) or along steep slopes or canyon head scarps (for instance, Ceramicola et al., 2014, Ionian sea) to date, the most relevant mass movements along the eastern Tyrrhenian margin are the "Nicotera" and "Villafranca" slides respectively 30 and 46 km^3 in volume, recognized in the Gioia basin, close to the Calabrian arc (Gamberi et al., 2011; Rovere et al., 2014), in a region mainly characterized by active tectonics and high seismicity rate.

5.2.2. Volcano-related process

The evidence that the ILC affects the apron of an active volcano seems far from casual and leads us to search for connections with the Island's volcanic history and behaviour. It is widely recognized that the post-55 ka resurgence of the Mt. Epomeo block in the central sector of Ischia Island has functioned principally through a series of co-seismic faults that border the block itself. Recent geological data would further suggest that such resurgence ceased at 5 ka (Sbrana et al., 2018) and that Mt. Epomeo is collapsing (Carlino et al., 2022), although this

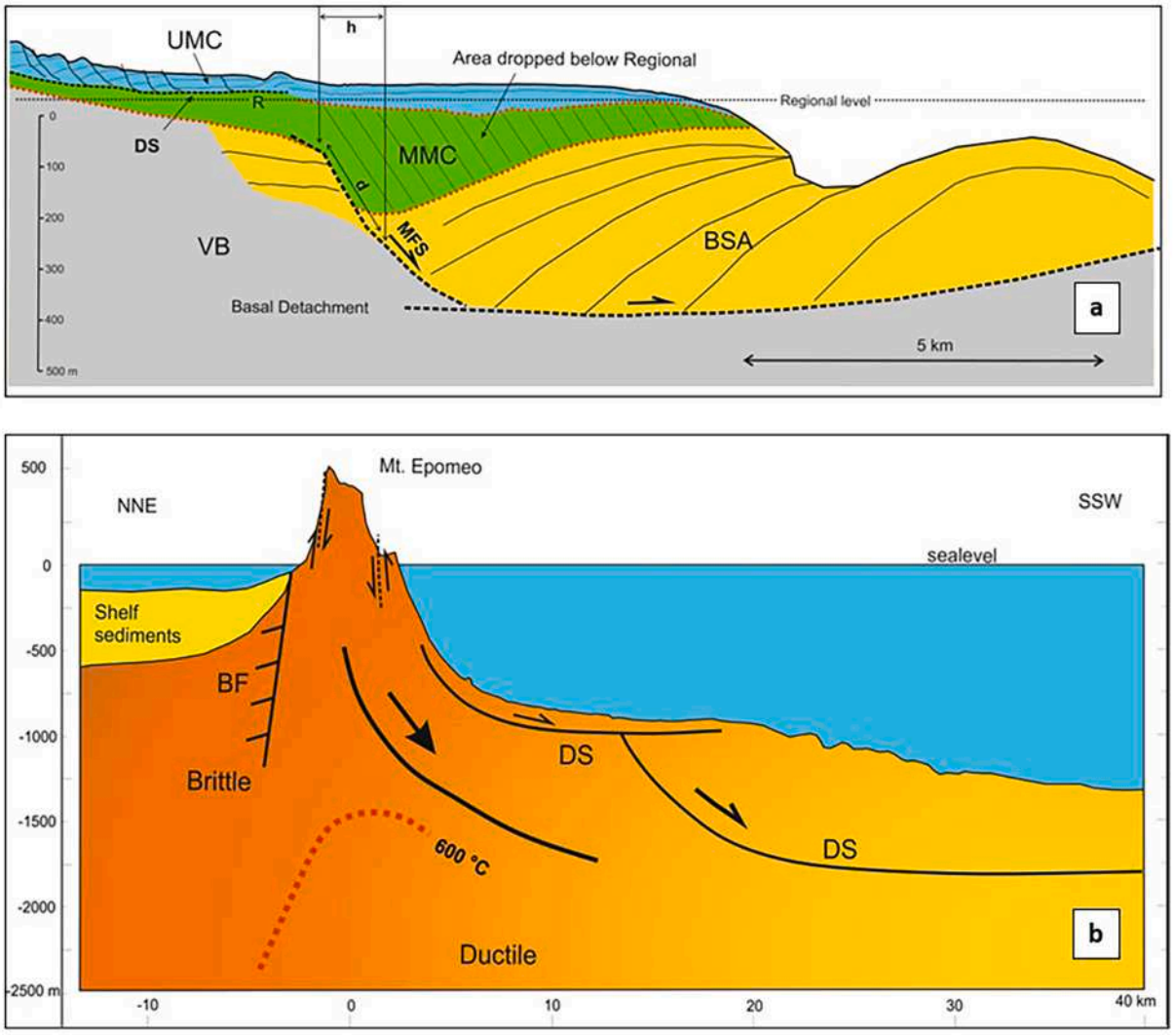

Fig. 15.. a) Scheme of the internal anatomy of ILC derived from seismo-stratigraphy and main parameters used for calculating the depth to detachment of listric faults described in the text; VB: volcanic basement; BSA: Basal Slump Anticline; MMC: Mid Mass-Movement complex; UMC: Upper Mass-Movement complex; DS: shallow detachment surface; LF: failure surface; h: heave; d: displacement. Dashed red lines are the main unconformities, dashed black lines are listric faults and their detachments. b) NNE-SSW section across Ischia island and its apron (approximate vertical exaggeration: 1:9) and concept of gravitational spreading favoured by a ductile rising basement. Brittle faults affetcting the Mt. Epomeo block are outlined. DS: Detachment Surfaces. BF: Buttressed northern Island's flank. Brittle and ductile domains and the 600 °C isotherm slightly modified after Castaldo et al., 2017.(For interpretation of the references to color in this figure legend, the reader is referred to the web version of this article.)

item is still debated. Whatever the dynamics of this rigid block, there is much evidence to suggest that it overlaps with long-term subsidence. Friedlander (1938) first observed at least 2 m of ground subsidence in the past 2 ka in specific coastal sectors of the Island based on underwater archaeological findings. More recently, precise ground levelling, spaceborne radar interferometry and 20 years of GPS observations indicate that almost all sectors of the Island are subsiding. Notably, subsidence rates up to 8 and 11 mm y^{-1} have been reported in the southern and northwestern flanks of Mt. Epomeo and even on its summit based on ground levelling (Del Gaudio et al., 2011) and interferometry (Manzo et al., 2006) while similar values ranging between 3 and 6 mm y^{-1} have been reported respectively to the east and the north of Mt. Epomeo block based on 20 years GPS observations (De Martino et al., 2021). This evidence indicates that, apart from local episodes of uplift around Mt. Epomeo, an overall subsidence trend embracing practically the entire volcanic complex can be recognized. Long-term subsidence and/or surface displacements detected in the edifice's upper section, together with the active growth of the slump fold along the undersea flank, can support a directional spreading hypothesis for the Ischia volcanic complex.

Several active continental strato-volcanoes (van Wyk de Vries et al., 2001; Borgia and van Wyk de Vries, 2003) or more significant oceanic shield edifices (Owen et al., 1995; Morgan et al., 2000, 2007) affected by volcanic spreading summit subsidence has been correlated to flank deformation. This is also the case at the summit of the Etna volcano, where subsidence of 1 m occurred from 1975 to 2000 was correlated with the growth of an anticline beneath Catania at a rate of 0.015 mm y^{-1} (Murray, 1994; Borgia et al., 2000). At Somma-Vesuvius volcano,

based on radar satellite interferometry and analogue/numeric modelling De Matteo et al., 2022report subsidence on the summit as opposed to a general uplift on the flanks and suggest a spreading-sagging behaviour. This series of cases, however, further indicates the distance between the complexity of nature and theoretical models and the need to introduce hybrid versions of them. For instance, a pure spreading model would prescribe contraction (thrusting, folding) at the base of the edifice, which would contradict the extensional regime we found on the Ischia slump, at least as far as we explored it. At the same time, the sagging behaviour, which should not be confused with volcano-tectonic subsidence due to site-specific factors (for Ischia, see Sepe et al., 2007), would prescribe contraction of the overall entire edifice and extensional (flexural) troughs far away from it.

In this case study, the volcano-sedimentary apron of the Ischia edifice has been deformed and partially detached from the footwall above a headscarp (listric) surface. This surface soles out on a nearly flat detachment located at about 400 m sub-bottom depth (Fig. 15a). Instability then has propagated upslope, promoting slope-parallel, relatively shallow detachments. A similar scenario, related to a larger-scale basaltic strato-volcano, has been proposed along the continental margin off Etna volcano, where a prominent undersea bulge, affected by curved extensional fault scarps, is the result of large-scale gravity instability that has propagated upslope promoting the downward sliding of the volcano's eastern flank (Chiocci et al., 2011).

Large hydrothermally altered volumes of volcanic rock in the central part of a volcano can produce low strength levels considered as potential failure surfaces for landslides and are thought to generate flank spreading and edifice deformation and destabilization (Merle and Lenat, 2003; Cecchi et al., 2005). Thus, in contrast to large oceanic counterparts where the basal detachment chiefly coincides with pelagic sediments and subordinately hyaloclastites and/or volcaniclastic deltas (Oehler et al., 2005), at Ischia volcano, the detachments may correspond to hydrothermally altered levels that pervasively affect the entire edifice. However, the lack of data on fluid emissions undersea other than hydrothermal vents located along the southern shore of the Island does not allow this hypothesis to be supported.

Regarding the thermal state inside Ischia volcano, Carlino et al. (2014), based on modelling and geothermal well data, propose a depth of 2000 m bsl for the top of the magmatic reservoir with a well-developed geothermal system extending above the reservoir up to shallow depths with average gradients of 150 to 225 °C km-1. Later Castaldo et al. (2017), based on thermo-rheological modelling, suggest the presence of an upper magmatic intrusion of 600 °C and a brittle/ductile transition, respectively, at −1500 m and 2500 m bsl, below the centre of the Island, with subsidence of the edifice at rates of 0.2–0.6 cm/y. These thermal models further support a still tentative, working hypothesis of a southward-directed spreading of the southern flank of the edifice and its volcano-sedimentary apron, provided that the northern flank is buttressed (Fig. 15b).

6. Conclusions

The integrated analysis of high-resolution geophysical and geological data acquired in the southern offshore of Ischia Island highlights that a sector of the southern submarine, volcano-sedimentary apron off Ischia Island, here named Ischia Landslide Complex (ILC), has undergone a large-scale failure with different types of mass movements. The ILC spreads from NNE to SSW until up to 40 km from the Island's coast; it barely exceeds 12 km in width over an area of 330 km^2. Its distal lobe attains 1400 m bsl.

The ILC is a composite depositional body consisting of the following members that seem genetically related to each other: 1) a very broad deep-seated slump anticline (BSA) with fanning strata and a tongue-shaped toe in the internal and external sector, respectively; 2) an intermediate-mass movement complex that formed into the morphological low created in the internal sector of the BSA, and 3) an upper mass movement complex resulting from intermittent debris flow and turbidite events alternating with hemipelagic deposition, partly remobilized by shallow slumping. Depth to detachment has been calculated between 350 and 450 m below the regional level. An overall volume of at least 50 km^3 of mobilized sediments can be assigned to the entire landslide complex, of which BSA represents 80% of the total.

The main basal slump deformation has started during the early construction of the Island's basement (Mid-Late Pleistocene) and has been partly coeval with one of the most voluminous and energetic eruptive cycle of Ischia volcanic complex between 75 and 33 ka. After that, the main phase of the deformation ILC motion did not cease but was still active. This evidence suggests a causal link with the present-day subsidence of the Island in the context of a directional spreading hypothesis.

Funding

This work was supported by the project ITHACA (ITaly HAzard from CApable faults), funded by Italian Institute for Environmental Protection and Research (ISPRA).

CRediT authorship contribution statement

Giovanni de Alteriis: Writing – original draft, Data curation, Conceptualization. **Crescenzo Violante:** Investigation, Funding acquisition, Data curation, Conceptualization. **Fabrizio Pepe:** Writing – review & editing, Formal analysis, Data curation.

Declaration of competing interest

The authors declare that they have no known competing financial interests or personal relationships that could have appeared to influence the work reported in this paper.

Data availability

Data will be made available on request.

Acknowledgments

We are grateful to all the crewmembers of the R/V Urania and the technical staff for their significant contribution to the geophysical survey operations during the 2010 cruise. Finally, we thank the editor and two anonymous reviewers for their comments and suggestions that have improved the manuscript.

References

Acocella, V., Funiciello, R., 2006. Transverse systems along the extensional Tyrrhenian margin of Central Italy and their influence on volcanism. Tectonics 25, TC2003. https://doi.org/10.1029/2005TC001845.

de Alteriis, G., Violante, C., 2009. Catastrophic landslides off Ischia volcanic island (Italy) during pre-history. In: Violante, C. (Ed.), Geo-hazard in Rocky Coastal Areas, 322. Geological Society, London, Special Publications, pp. 73–104.

de Alteriis, G., Insinga, D., Morabito, S., Morra, V., Chiocci, F.L., Terrasi, F., Lubritto, C., Di Benedetto, C., Pazzanese, M., 2010. Age of submarine debris avalanches and tephrostratigraphy offshore Ischia Island, Tyrrhenian Sea, Italy. Mar. Geol. 278, 1–18. https://doi.org/10.1016/j.margeo.2010.08.004.

Borgia, A., van Wyk de Vries, B., 2003. The volcano-tectonic evolution of Concepción, Nicaragua. Bull. Volcanol. 65, 248–266.

Borgia, A., Ferrari, L., Pasquaré, G., 1992. Importance of lateral spreading in the tectonic and volcanic evolution of Mount Etna. Nature 357, 231–235.

Borgia, A., Lanari, R., Sansosti, E., Tesauro, M., Berardino, P., Fornaro, G., Neri, M., Murray, J.B., 2000. Actively growing anticlines beneath Catania from the distal motion of Mount Etna's decollement measured by SAR interferometry and GPS. Geophys. Res. Lett. 27 (20), 3409–3412.

Brown, R.J., Orsi, G., de Vita, S., 2008. New insights into late Pleistocene explosive volcanic activity and caldera formation on Ischia (southern Italy). Bull. Volcanol. 70, 583–603. https://doi.org/10.1007/s00445-007-0155-0.

Bruno, P.P., de Alteriis, G., Florio, G., 2002. The western undersea section of the Ischia volcanic complex (Italy, Tyrrhenian Sea) inferred from marine geophysical data. Geophys. Res. Lett. 29, 1029–1034.
Budillon, F., Cesarano, M., Conforti, A., Pappone, G., Di Martino, G., Pelosi, N., 2014. Recurrent superficial sediment failure and deep gravitational deformation in a Pleistocene slope marine succession: the Poseidonia slide (Salerno Bay, Tyrrhenian sea). In: Krastel, S., et al. (Eds.), Submarine Mass Movements and Their Consequences, Advance in Natural and Technological Hazard Research, vol. 37, pp. 273–284.
Byrne, P.K., Holohan, E.P., Kervyn, M., van Wyk de Vries, B., Troll, V.R., Murray, J.B., 2013. A sagging-spreading continuum of large volcano structure. Geology 41, 339–342.
Carlino, S., Somma, R., Troiano, A., Di Giuseppe, M.G., Troise, C., De Natale, G., 2014. The geothermal system of Ischia Island (southern Italy): critical review and sustainability analysis of geothermal resource for electricity generation. Renew. Energy 62, 177–196.
Carlino, S., Sbrana, A., Pino, N.A., Marianelli, P., Pasquini, G., De Martino, P., De Novellis, V., 2022. The volcano-tectonics of the northern sector of Ischia Island caldera (Southern Italy): resurgence, subsidence and earthquakes. Front. Earth Sci. 10, 1–16. https://doi.org/10.3389/feart.2022.730023.
Castaldo, R., Gola, G., Santilano, A., De Novellis, V., Pepe, S., Manzo, M., Manzella, A., Tizzani, P., 2017. The role of thermo-rheological properties of the crust beneath Ischia Island (Southen Italy) in the modulation of the ground deformation pattern. J. Volcanol. Geotherm. Res. 344, 154–173. https://doi.org/10.1016/j.jvolgeores.2017.03.003.
Cecchi, E., van Wyk de Vries, B., Lavest, J.M., 2005. Flank spreading and collapse of weak-cored volcanoes. Bull. Volcanol. 67, 72–91. https://doi.org/10.1007/s00445-004-0369-3.
Ceramicola, S., Praeg, D., Coste, M., Forlin, E., Cova, A., Colizza, E., Critelli, S., 2014. Submarine mass-movements along the slopes of the active Ionian continental margins and their consequences for marine geo-hazards (Mediterranean Sea). In: Submarine Mass Movements and theis Consequences. Springer International Publishing, pp. 295–306.
Chiocci, F.L., de Alteriis, G., 2006. The Ischia debris avalanche. First, clear submarine evidence in the Mediterranean of a volcanic island pre-historic collapse. Terra Nova 18, 202–209.
Chiocci, F.L., Coltelli, M., Bosman, A., Cavallaro, D., 2011. Continental margin large-scale instability controlling the flank sliding of Etna volcano. Earth Planet. Sci. Lett. 305, 57–64.
Chiocci, F.L., Budillon, F., Ceramicola, S., Gamberi, F., Orrù, P., 2021. Atlante dei Lineamenti di Pericolosità Geologica dei mari italiani – Risultati del Progetto MaGIC. CNR edizioni, Roma.
Conti, A., Bigi, S., Cuffaro, M., Doglioni, C., Scrocca, D., Muccini, F., Cocchi, L., Ligi, M., Bortoluzzi, G., 2017. Transfer zones in an oblique back-arc basin setting: insights from the Latium-Campania segmented margin (Tyrrhenian Sea). Tectonics 36, 78–107. https://doi.org/10.1002/2016TC004198.
Corredor, F., Shaw, J.H., Bilotti, F., 2005. Structural styles in thedeep-water fold and thrustbelts of the Niger Delta. AAPG Bull. 89 (6), 753–780.
De Martino, P., Dolce, M., Brandi, G., Scarpato, G., Tammaro, U., 2021. The ground deformation history of the Neapolitan Volcanic Area (Campi Flegrei Caldera, Somma–Vesuvius Volcano, and Ischia Island) from 20 Years of Continuous GPS Observations (2000–2019). Remote Sens. 2021 (13), 2725. https://doi.org/10.3390/rs13142725.
De Matteo, A., Massa, B., Castaldo, R., D'Auria, L., James, M.R., Lane, S.J., Pepe, S., Tizzani, P., 2022. An integrated modeling approach for analyzing the deformation style of active volcanoes: Somma-Vesuvius case-study. J. Geophys. Res. 127 https://doi.org/10.1029/2021JB022338.
Del Gaudio, C., Aquino, I., Ricco, C., Sepe, V., Serio, C., 2011. Geodetic Surveillance of the Ischia Island: results of the Precision Levelling performed in June 2010. Quader. Geof. 2011, 87.
Delaney, P.T., Denlinger, R.P., Lisowski, M., Miklius, A., Okubo, P.G., Okamura, A.T., Sako, M.K., 1998. Volcanic spreading at Kilauea, 1976–1996. J. Geophys. Res. 103 (B8), 18003–18023. https://doi.org/10.1029/98JB01665.
Delcamp, A., van Wyk de Vries, B., James, M.R., 2008. The influence of edifice slope and substrata on volcano spreading. J. Volcanol. Geotherm. Res. 177, 925–943. https://doi.org/10.1016/j.jvolgeores.2008.07.014.
Delcamp, A., van Wyk de Vries, B., James, M.R., Gailler, L.S., Lebas, E., 2012. Relationships between volcano gravitational spreading and magma intrusion. Bull. Volcanol. 74, 743–765. https://doi.org/10.1007/s00445-011-0558-9.
Della Seta, M., Marotta, E., Orsi, G., de Vita, S., Sansivero, F., Fredi, P., 2012. Slope instability induced by volcano-tectonics as an additional source of hazard in active volcanic areas: the case of Ischia island (Italy). Bull. Volcanol. 74, 79–106. https://doi.org/10.1007/s00445-011-0501-0.
Denlinger, R.P., Okubo, P., 1995. Structure of the mobile south flank of Kilauea Volcano, Hawaii. J. Geophys. Res. 100 (B12), 24499–24507. https://doi.org/10.1029/95JB01479.
Di Napoli, R., Martorana, R., Orsi, G., Aiuppa, A., Camarda, M., De Gregorio, S., Gagliano Candela, E., Luzio, D., Messina, N., Bitetto, M., de Vita, S., Valenza, M., 2011. The structure of a hydrothermal system from an integrated geochemical, geophysical, and geological approach: the Ischia Island case study. Geochem. Geophys. Geosyst. 12, Q07017. https://doi.org/10.1029/2010GC003476.
Dula, W.F., 1991. Geometric models of listric normal faults and rollover folds. AAPG Bull. 75, 1609–1625.
Færseth, R., Sætersmoen, B.H., 2008. Geometry of a major slump structure in the Storegga slide region offshore western Norway. Nor. J. Geol. 88, 1–11.
Frey-Martinez, J., Cartwright, J., Hall, B., 2005. 3D seismic interpretation of slump complexes: examples from the continental margin of Israel. Basin Res. 17, 83–108.
Friedlander, L., 1938. Sui bradisismi dell'isola d'Ischia e sulla Grotta del Mago. Bollet. della Soc. Geogr. Ital. Ser. VII 3 (1), 4–54.
Gamberi, F., Rovere, M., Marani, M., 2011. Mass-transport complex evolution in a tectonically active margin (Gioia Basin, Southeastern Tyrrhenian Sea). Mar. Geol. 279, 98–110.
Gillot, P.-Y., Chiesa, S., Pasquare, G., Vezzoli, L., 1982. 33.000 yr K/Ar dating of the volcano- tectonic horst of the isle of Ischia, Gulf of Naples. Nature 229, 242–245.
González, P.J., Tiampo, K.F., Camacho, A.G., Fernández, J., 2010. Shallow flank deformation at Cumbre Vieja volcano (Canary Islands): Implications on the stability of steep-sided volcano flanks at oceanic islands. Earth Planet. Sci. Lett. 297 (3), 545–557.
Holohan, E.P., Poppe, S., Delcamp, A., Byrne, P.K., Walter, T.R., van Wyk de Vries, B., Kervyn, M., 2023. Transition from volcano-sagging to volcano-spreading. Earth Planet. Sci. Lett. 604, 118012 https://doi.org/10.1016/j.epsl.2023.118012.
Hühnerbach, V., Masson, D.G., COSTA project partners, 2004. Landslides in the North Atlantic and its adjacent seas: an analysis of their morphology, setting and behaviour. Mar. Geol. 213, 343–362. https://doi.org/10.1016/j.margeo.2004.10.013.
Kervyn, M., van Wyk de Vries, B., Walter, T.R., Njome, M.S., Suh, C.E., Ernst, G.G.J., 2014. Directional flank spreading at Mount Cameroon volcano: evidence from analogue modeling. J. Geophys. Res. Solid Earth 119, 7542–7563. https://doi.org/10.1002/2014JB011330.
Le Corvec, N., Walter, T.R., 2009. Volcano spreading and fault interaction influenced by rift-zone intrusions: Insights from analogue experiments analyzed with digital image correlation. J. Volcanol. Geotherm. Res. 183 (3–4), 170–182. https://doi.org/10.1016/j.jvolgeores.2009.02.006.
Malinverno, A., Ryan, W.B.F., 1986. Extension in the Tyrrhenian Sea and shortening in the Apennines as result of arc migration driven by sinking of the lithosphere. Tectonics 5, 227–245. https://doi.org/10.1029/TC005i002p00227.
Manzo, M., Ricciardi, G.P., Casu, F., Ventura, G., Zeni, G., Borgström, S., Berardino, P., Del Gaudio, C., Lanari, R., 2006. Surface deformation analysis in the Ischia Island (Italy) based on spaceborne radar interferometry. J. Volcanol. Geotherm. Res. 151, 399–416.
Marani, M., Gamberi, F., 2004. Structural framework of the Tyrrhenian Sea unveiled by seafloor morphology. In: Marani, M.P., Gamberi, F., Bonatti, E. (Eds.), From Seafloor to Deep Mantle: Architecture of the Tyrrhenian Back-Arc Basin: Mem. Descr. Carta Geol. It., v. 44. Roma, System Cart, pp. 97–108.
Masson, D.G., Harbitz, C.B., Wynn, R.B., Pedersen, G., Løvholt, F., 2006. Submarine landslides: processes, triggers and hazard prediction. Phil. Trans. R. Soc. A 364, 2009–2039.
McGovern, P.J., Grosfils, E.B., Galgana, G.A., Morgan, J.K., Rumpf, M.E., Smith, J.R., Zimbelman, J.R., 2015. Lithospheric flexure and volcano basal boundary conditions: keys to the structural evolution of large volcanic edifices on the terrestrial planets. Geol. Soc. Lond. Spec. Publ. 401, 219–237. https://doi.org/10.1144/sp401.7.
Merle, O., Lenat, J.F., 2003. Hybrid collapse mechanism at Piton de la Fournaise volcano, Reunion Island, Indian Ocean. J. Geophys. Res. 108 (B3), 2166. https://doi.org/10.1029/2002JB002014. 2003.
Milia, A., Torrente, M.M., 1999. Tectonics and stratigraphic architecture of a peri-Tyrrhenian half-graben (Bay of Naples, Italy). Tectonophysics 315, 301–318.
Milia, A., Aiello, G., Iannace, P., Torrente, M.M., 2021. Complex stratigraphic relationships between volcanic features and sedimentary deposits in a submarine environment: the northern offshore Holocene Ischia volcanic field (Italy). J. Volcanol. Geotherm. Res. 419, 107379 https://doi.org/10.1016/j.jvolgeores.2021.107379.
Mitchell, N.C., Masson, D.G., Watts, A.B., Gee, M.J.R., Urgeles, R., 2002. The morphology of the submarine flanks of volcanic ocean islands: a comparative study of the Canary and Hawaiian hotspot islands. J. Volcanol. Geotherm. Res. 115, 83–107.
Moore, J.G., Normark, W.R., Holcomb, R.T., 1994. Giant Hawaiian Landslides. Annu. Rev. Earth Planet. Sci. 22, 119–144.
Morgan, J.K., Moore, G.F., Hills, D.J., Leslie, S., 2000. Overthrusting and sediment accretion along Kilauea's mobile south flank, Hawaii: evidence for volcanic spreading from marine reflection data. Geology 28, 667–670.
Morgan, J.K., Clague, D.A., Borchers, D.C., Davis, A.S., Milliken, K.L., 2007. Mauna Loa's submarine western flank: Landsliding, deep volcanic spreading, and hydrothermal alteration. Geoch-Geoph-Geos 8 (5), 1–42. https://doi.org/10.1029/2006GC001420.
Mulder, T., Cochonat, P., 1996. Classification of offshore mass movements. J. Sediment. Res. 66, 43–57.
Murray, J.B., 1994. Elastic model of the actively intruded dyke feeding the1991-1993 eruption of Mt Etna, derived from ground deformation measurements. Acta Vulcanol. 4, 97–99.
Oehler, J.F., Van, W.D.V.B., Labazuy, P., 2005. Landslides and spreading of oceanic hotspotand arc shield volcanoes on low strength layers (LSLs); an analogue modeling approach. J. Volcanol. Geotherm. Res. 144 (1–4), 169–189.
Orsi, G., Gallo, G., Zanchi, A., 1991. Simple shearing block-resurgence in caldera depression. A model from Pantelleria and Ischia. J. Volcanol. Geotherm. Res. 47, 1–11.
Owen, S., Segall, P., Freymueller, J., Miklius, A., Denlinger, R., Arnadottir, T., Sako, M., Burgmann, R., 1995. Rapid deformation of the south flank of Kilauea volcano, Hawaii. Science 267, 1328–1332.
Poblet, J., Bulnes, M., 2005. Fault-slip, bed-length and area variations in experimental rollover anticlines over listric normal faults: influence in extension anddepth to detachment estimations. Tectonophysics 396, 97–117.

Poland, M.P., Peltier, A., Bonforte, A., Puglisi, G., 2017. The spectrum of persistent volcanic flank instability: a review and proposed framework based on Kilauea, Piton de la Fournaise, and Etna. J. Volcanol. Geotherm. Res. 339, 63–80.

Romeo, S., D'Angiò, D., Fraccica, A., Licata, V., Vitale, V., Chiessi, V., Amanti, M., Bonasera, M., 2023. Ivestigation and preliminary assessment of the Casamicciola landslide in the Island of Ischia (Italy) on November 26, 2022. Landslides. https://doi.org/10.1007/s10346-023-02064-0.

Rovere, M., Gamberi, F., Mercorella, A., Leidi, E., 2014. Geomorphometry of a submarine mass-transport complex and relationships with active faultsina rapidly uplifting margin (Gioia Basin, NE Sicily margin). Mar. Geol. 356, 31–43.

Sbrana, A., Marianelli, P., Pasquini, G., 2018. Volcanology of Ischia (Italy). J. Maps 14 (2), 494–503.

Sepe, V., Atzori, S., Ventura, G., 2007. Subsidence due to crack closure and depressurization of hydrothermal systems: a case study from Mt Epomeo(Ischia Island, Italy). Terranova 19, 127–132.

Tibaldi, A., Vezzoli, L., 2004. A new type of volcano flank failure: the resurgent caldera sector collapse, Ischia, Italy. Geophys. Res. Lett. 31, L14605 https://doi.org/10.1029/2004GL020419.

Vezzoli, L., 1988. Island of Ischia. Quaderni de 'La Ricerca Scientifica' Progetto finalizzato 'Geodinamica'. CNR Monogr. Final. 10.

Violante, C., Budillon, F., Esposito, E., Porfido, S., Vittori, E., 2004. Submerged hummocky topographies and relations with landslides on the northwestern flank of Ischia island, southern Italy. In: Patron Editore, Proceedings of "Occurrence and Mechanisms of FLOW-like Landslides in natural Slopes and Earthfills", Sorrento, 14–16 May 2003. Associazione Geotecnica Italiana, Bologna, pp. 309–315.

de Vita, S., Sansivero, F., Orsi, G., Marotta, E., Piochi, M., 2010. Volcanological and structural evolution of the Ischia resurgent caldera (Italy) over the past 10 k.y. In: Groppelli, G., Viereck-Goette, L. (Eds.), Stratigraphy and Geology of Volcanic Areas: Geological Society of America Special Paper, vol. 464, pp. 193–241. https://doi.org/10.1130/2010.2464(10).

van Wyk de Vries, B., Self, S., Francisc, P.W., Keszthelyid, L., 2001. A gravitational spreading origin for the Socompa debris avalanche. J. Volcanol. Geotherm. Res. 105, 225–247.